



Faculty of Science and Technology

MASTER THESIS

Study program/Specialization: Study program - Construction and Materials Specialization - Offshore Constructions	Vårsemesteret, 2016 Open / Restricted access
Writer: Tord Slåke	 (Writer's signature)
Faculty supervisor: Sudath C. Siriwardane and Ove Mikkelsen External supervisor(s): Patrick Decosemaker	
Thesis title: Analysis of Jacket type fixed platforms – Effect of various mass modelling approaches for Topsides on structural response	
Credits (ECTS): 30 poeng	
Key words: - Wave theories - Finite element analysis - SAP 2000 - Mass modelling	 Pages: 72 Stavanger, 15.06.2016

Abstract

A fixed platform in shallow waters is supported on a Jacket structure with a heavy Topside over it. The Jacket design is designed for various limit states including the ultimate limit state (ULS), serviceability limit state (SLS) and the fatigue limit state (FLS). The loading on a Jacket is generally the environmental loading and gravity loads. The environmental loads are wind, wave and current loading. The wave loading is generally governing and wave theory used in analysis need to be chosen carefully. The gravity loads are from the overhead Topside in addition to self-weight of the Jacket. It is observed in some cases that while the Jacket design is completed, the Topsides work including some part on the design is not completed. Also many a times the Topside and Jacket design contracts are given out to separate engineering contractors depending on their expertise and specialized experience. For Jacket contractors, it becomes not only impractical but also uneconomical to spend hundreds of hours on modelling the Topside in minute detail. In such cases it is very important to represent the Topside mass precisely for the Jacket design.

However, not many guidelines are available on the mass modelling approaches to be adopted for Topside modelling in cases where limited information and time is available. Various approaches of modelling the Topside mass are formulated and discussed in this thesis. These approaches are first demonstrated on a simple structure. The approaches are then used for a case study on one of the heaviest offshore structure in the Norwegian Continental Shelves (NCS). The Topside has a weight of 28000 tons in this case. The results using various approaches are presented and conclusions are drawn. In the end, recommendations are made for practicing engineers on adopting suitable approach for modelling the Topside in case of lack of detailed information or lack of time. A case study on the effect of wave theory on the structural response of the Jacket structure is also performed and results are presented.

Acknowledgement

This thesis is the final work that concludes my master degree in Mechanical and Structural Engineering with specialization in Offshore Construction at the University of Stavanger, Norway. The subject of this thesis was proposed in collaboration with my supervisor Prof. S.A. Sudath C Siriwardane. This thesis work is carried out at University of Stavanger, Norway in period January 2016 to June 2016.

I wish to express my deep gratitude for the support and help offered by the following individuals in completing this thesis. First, I would to thank my supervisor Prof. S. A. Sudath C Siriwardane for constructive feedbacks, guidance and advice throughout the thesis work. I would also like to thank Associate Prof. Ove Mikkelsen for general discussion and positive feedbacks during this work. I will also like to thank Patrick Decosemaker from TOTAL for providing me information for the considered case study. Lastly, I would like to thank Research Fellow Ashish Aeran for his large impact on my work. He has guided me from early stages of this thesis and always made sure that I understood everything that I was supposed to do.

Stavanger, 15th June 2016.

Tord Slåke

Table of Contents

1. Introduction	1
1.1. Background.....	1
1.2. Martin Linge platform	3
1.3. Motivation and objectives	4
1.4. Organization of the report.....	5
2. Wave theories and underlying assumptions	6
2.1. Assumptions, basic equations and boundary conditions	6
2.2. Airy’s linear theory.....	8
2.3. Stokes nonlinear wave theory.....	9
2.4. Validity regions of various wave theories	9
3. FEM modelling and analysis	12
3.1. General.....	12
3.2. SAP2000.....	12
3.3. Design parameters	12
3.3.1. Waves.....	13
3.3.2. Current.....	13
3.4. Modal Analysis.....	14
3.4.1. Eigenvector analysis.....	14
3.5. ULS and SLS analysis	16
3.5.1. Ultimate limit state (ULS).....	16
3.5.2. Serviceability limit state (SLS).....	16
4. Case study part 1: Effect of wave theory on analysis.....	17
4.1. Analysis on a simple column.....	17
4.1.1. Analysis in SAP2000 using linear Airy’s wave theory.....	17
4.1.2. Manual calculations using linear wave Theory	18
4.1.1. Comparison of SAP2000 and manual calculations	21
4.2. Analysis of complex Jacket structure	22
4.2.1. Structural model	22
4.2.2. Structural analysis – Natural frequencies, SLS and ULS.....	27
4.2.3. Loading conditions – Load cases and combinations	27
4.2.4. Analysis results – Natural frequencies	28
4.2.5. Analysis results – Leg displacements (SLS).....	29

4.2.6.	Analysis results – Member capacity check (ULS)	32
5.	Case study – Part 2: Mass modelling approaches	33
5.1.	Mass modelling approaches.....	33
5.2.	Mass modelling approaches demonstration on simple beam	34
5.2.1.	Section and material properties	34
5.2.2.	Mass modelling approaches and analysis in SAP2000 - 2 nodes	34
5.2.3.	Mass modelling approaches and analysis in SAP2000 - 6 nodes	36
5.2.4.	SAP2000 results comparison with numerical and analytical solution	38
5.3.	Mass modelling approaches demonstration on Martin Linge Topside.....	41
5.3.1.	Topside models developed using mass modelling approaches	41
5.3.2.	Results – Eigenvalue analysis	46
5.3.3.	Results – Serviceability limit state (SLS)	47
5.3.4.	Results – Ultimate limit state (ULS).....	47
6.	Discussion and Conclusions.....	52
6.1.	Discussion and Conclusions	52
6.2.	Scope of future work	54
7.	References	55
 APPENDIX A - Analytical calculations for simple beam.....		56
 APPENDIX B - MATLAB code for 6 node beam (2D element).....		58
 APPENDIX C – CoG calculations for the Topside modules.....		62

List of Figures

Figure 1-1 First installed oil platform in the Gulf of Mexico [1].....	1
Figure 1-2 Offshore platform development [2].....	1
Figure 1-3 Location of Hild field in NCS region	3
Figure 1-4 Conceptual image for Martin Linge platform in the Hild oil field.....	3
Figure 1-5 Martin Linge Jacket transportation offshore	4
Figure 1-6 Martin Linge Jacket installation on the site.....	4
Figure 2-1 Qualitative representation of a linear wave form (dashed) vs Stokes wave (dotted) ...	10
Figure 2-2 Validity range of various wave theories	11
Figure 4-1 Wave profile and horizontal particle velocity from SAP2000	18
Figure 4-2 3D Jacket model in SAP2000.....	22
Figure 4-3 line model of Jacket in SAP2000	22
Figure 4-4 Jacket model in XZ plane	23
Figure 4-5 Jacket model in YZ plane	23
Figure 4-6 Topside drawing received from TOTAL.....	24
Figure 4-7 Topside drawing received from TOTAL.....	25
Figure 4-8 Topside model in SAP2000.....	25
Figure 4-9 Topside and Jacket model in SAP2000	26
Figure 4-10 Considered leg A of the Jacket.....	29
Figure 4-11 Leg A displacement U1 (x-direction) using nonlinear wave theory	30
Figure 4-12 Leg A displacement U1 (x-direction) using linear Airy's wave theory	30
Figure 4-13 Leg A displacement U1 comparison between linear and nonlinear wave theory	30
Figure 4-14 Leg A displacement U2 (y-direction) using nonlinear wave theory	31
Figure 4-15 Leg A displacement U2 (y-direction) using linear Airy's wave theory	31
Figure 4-16 Leg A displacement U1 comparison between linear and nonlinear wave theory	31
Figure 4-17 Utilization ratio in members using nonlinear 5 th order Stokes wave theory	32
Figure 4-18 Utilization ratio in members using linear Airy's wave theory	32
Figure 5-1 Considered cantilever beam	34
Figure 5-2 Considered cantilever beam	34
Figure 5-3 Mode shapes for the considered cantilever beam.....	39

Figure 5-4 First 5 natural frequencies comparison.....	39
Figure 5-5 Mode 5 to mode 10 natural frequencies comparison.....	40
Figure 5-6 Error percentage in various approaches	40
Figure 5-7 Topside model for density increment approach	42
Figure 5-8 Topside mass representation for approach 2	43
Figure 5-9 Topside mass representation for approach 2	43
Figure 5-10 Topside model for lumped mass approach case 1	44
Figure 5-11 Complete model for lumped mass approach case 1	44
Figure 5-12 Complete model for lumped mass approach case 1	44
Figure 5-13 Topside model for lumped mass approach case 2	45
Figure 5-14 Complete model for lumped mass approach case 2	45
Figure 5-15 Natural time period for various mass modelling approaches – global modes.....	46
Figure 5-16 Leg A displacement U1 for various approaches – worst load combination.....	47
Figure 5-17 Leg A displacement U2 for various approaches – for worst load combination	47
Figure 5-18 UC plot for Jacket – density increment approach	48
Figure 5-19 UC plot for Jacket – point loads approach	49
Figure 5-20 UC plot for Jacket – lumped mass approach case 1	50
Figure 5-21 UC plot for Jacket – lumped mass approach case 2	51

List of Tables

Table 3-1 Wave parameters.....	13
Table 3-2 Surface current for 100 year return period.....	13
Table 3-3 Vertical current profile for 100 year return period	14
Table 3-4 Limit states and corresponding factors	16
Table 4-1 Section and material properties of column	17
Table 4-2 Drag and inertia coefficients are taken as per API	18
Table 4-3 Water depth relation with frequency	19
Table 4-4 Iteration for calculation for k	19
Table 4-5 Calculation of horizontal particle velocity.....	20
Table 4-6 Weight comparison between platform x Topside and Martin Linge Topside	24
Table 4-7 Density factor for various modules of Martin Linge Topside	27
Table 4-8 Load combinations considered in the ULS analysis	28
Table 4-9 Load combinations considered in the SLS analysis.....	28
Table 4-10 Natural periods and vibration modes for the Jacket model	29
Table 4-11 Unity check values of critical members of Jacket	32
Table 5-1 Section and material properties of beam.....	34
Table 5-2 Mass modelling approaches demonstrated on a simple 2 node beam element.....	35
Table 5-3 Static displacement results for various approaches for 2 nodes case	35
Table 5-4 Natural frequency comparison for 2 node element (vertical plane only)	36
Table 5-5 Mass modelling approaches demonstrated on a simple 6 node beam element.....	36
Table 5-6 Static displacement results for various approaches for 6 nodes case	37
Table 5-7 Natural frequency comparison for 6 node element (vertical plane only)	37
Table 5-8 Frequency comparison of SAP2000 results with numerical and analytical solution	38
Table 5-9 Natural time period of structure in various approaches	46
Table 5-10 UC values for leg A in various approaches	47

1. Introduction

1.1. Background

The oil and gas industry has developed well over the last few decades. The offshore exploration began in the United States when Henry Williams began extracting oil from the Summerland field of the Californian coast near Santa Barbara in the 1890's. This platform is shown in Figure 1-1.

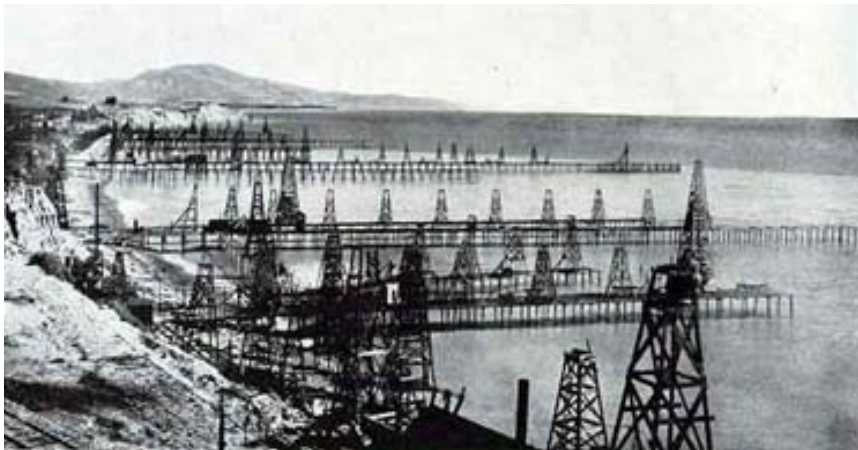


Figure 1-1 First installed oil platform in the Gulf of Mexico [1]

Since the installation of the first platform in the Gulf of Mexico, the offshore industry has seen many innovative structures placed in deeper waters and more hostile environment. Slowly and gradually by 1975, structures were installed in water depths until 475 ft (144m). By 1980s, the water depths increased significantly to more than 300m. The progress of platform development into deeper water is shown in Figure 1-2.

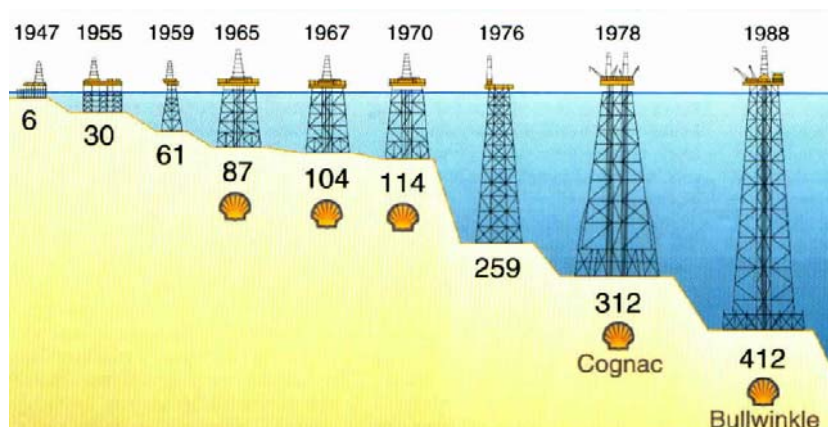


Figure 1-2 Offshore platform development [2]

Since 1947, more than 10000 offshore structures have been constructed and installed worldwide. A majority of these platforms are made of steel and are anchored to the sea floor using piles. These platforms are called fixed Jacket type platforms and will be the main focus for this thesis.

The above discussed fixed platforms are generally installed in shallow waters. Shallow water depths are generally until 300 to 400 meters. Beyond this depth, it is technically not possible to install fixed type platforms due to stability issues. Also, the oil reserves in deeper waters need to be extracted to meet rising energy demands. To counteract deeper waters, floating type structures were developed. Such floating structures can be jack-ups, floating ships, spars or semi-submersibles which are tied to the seabed using moorings.

A typical fixed platform has two main parts namely the Topsides and the supporting Jacket. While designing the Jacket for various limit states (SLS, ULS, FLS), it is important to consider all the possible loading on the structure. These loading are generally the gravity loads along with the environmental loading. The gravity loads are from the overhead Topside in addition to self-weight of the Jacket. The environmental loads are wind, wave and current loading.

The deadweight of the Topside is one of the governing criteria for the Jacket design. However, sometimes the Topside information is not fully available to the practicing engineers. This might be due to several reasons such as design contract only for the Jacket or lack of time to model the Topside in very detailed manner. This might also be due to the lack of complete Topside information from the second contractor designing the Topside. In such cases, it is very important to model the Topside in an approximate but correct manner without compromising on the precision of Jacket design. There can be various approaches to model the Topside mass.

Various approaches of modelling the Topside are formulated and discussed in this thesis. This is done through a case study on one of the heaviest offshore structure in the Norwegian Continental Shelves (NCS). The Topside has a weight of 28000 tons in this case. The results using various approaches are presented and conclusions are drawn. In the end, recommendations are made for practicing engineers on adopting suitable approach for modelling the Topside in case of lack of detailed information or lack of time. More details about the considered offshore platform is presented in the next section.

1.2. Martin Linge platform

Martin Linge is a Norwegian off-shore project, developed by TOTAL E&P Norway (51%) acting as operator with Petoro (30%) and Statoil (19%) as partners. Martin Linge is located in a field called Hild field and are in the North West part of the Norwegian Continental Shelves (NCS) approximately 170 km west of Bergen as shown in Figure 1-3. The field contains gas, condensate and oil discoveries at around 190 million barrels of oil equivalent. The conceptual design is shown in Figure 1-4.

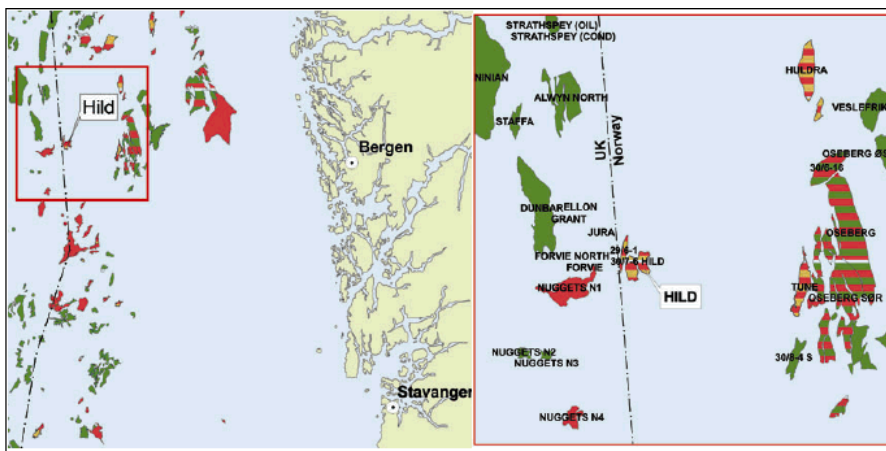


Figure 1-3 Location of Hild field in NCS region

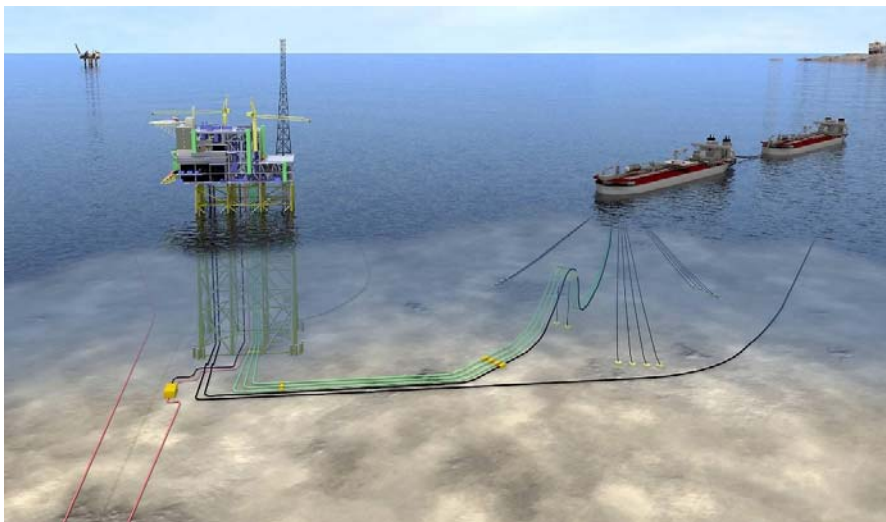


Figure 1-4 Conceptual image for Martin Linge platform in the Hild oil field

The Jacket is a fixed installation that consists of 8 main legs and mainly X-bracing between the six horizontal elevations. The Jacket is at a depth of 114 meters and will be supported to the seabed with the use of pile clusters that are located at the four bottom corners of the Jacket. These piles

have a dimension of 96 inches and the pile clusters contains 4 piles each with a total of 16 piles and a length of 65m each. The Jacket was transported on a barge and was launched and upended in the North Sea in 2014. Some of the images from the installation phase are shown in Figure 1-5 and Figure 1-6.



Figure 1-5 Martin Linge Jacket transportation offshore



Figure 1-6 Martin Linge Jacket installation on the site

The Topside was planned to be installed in 2016. However, the project is running behind schedule due to unforeseen delays. The Topside is currently under design and fabrication stage and is now expected to be installed in 2018.

1.3. Motivation and objectives

The motivation for this thesis came from the Martin Linge project. The platform has a Topside weighting 28000 ton and Jacket weighing 10000 tons. This is one of the heaviest in the NCS region. It is seen that while the Jacket is already been installed, the Topsides work including some part on design is still ongoing. In such cases it is very important to represent the Topside mass precisely for the Jacket design even when the Topside (and its modules) mass information is not available in detail. Also many a times the Topside and Jacket design contracts are given out to separate

engineering contractors depending on their expertise. In such cases, for the engineering contractor designing the Jacket, it becomes not only impractical but also uneconomical to spend many hours on modelling the Topside in minute detail. But at the same time it is important to represent the Topside mass as precise as possible to capture the structural response of the Jacket accurately. It is found that the currently available guidelines do not mention any procedures for modelling the Topside mass approximately without modelling each of its modules in detail. The motivation of this thesis is to consider various possible approaches of modelling a Topside mass given limited information and limited time.

A number of objectives are identified for this thesis. The first objective is to investigate the effect of various wave theories on the structural response of the Jacket structure. Analysis is performed for both linear and nonlinear wave theories. The study is first performed on a simple beam structure and results are compared with manual calculations to gain a good understanding. The study is then extended to the big Jacket structure and results are presented. The results are compared and conclusions are drawn. This study will be referred to as the first part of case study in future sections.

The second and main objective of this thesis is to investigate various approaches of modelling the Topside mass over the Jacket. The need of such approaches is generally required in the industry due to lack of information on the Topside data as well as due to lack of time. Various approaches are formulated and results are presented. In the end, conclusions are drawn and recommendations are made for practicing engineers on the selection of suitable approach for modelling the Topside mass. Again, the study is first conducted on a simple beam structure and results are verified with manual and analytical solution before moving ahead with the complex Jacket structure. This part of the study will be referred to as the second part of the case study in future sections.

1.4. Organization of the report

The thesis is organized in 6 chapters. Various wave theories and their underlying assumptions are discussed in chapter 2. Chapter 3 discusses about the FE modelling and analysis in FE software SAP 2000. The theory behind modal analysis and limit states analysis (SLS, ULS) is also presented. The first part of the case study is presented in Chapter 4 and it investigate the effect of various wave theories on the structural response of the Jacket. The second part of the case study is presented in Chapter 5 and various approaches of modeling the Topside mass is discussed in this chapter. Discussion, conclusion and scope of future work is presented in Chapter 6.

2. Wave theories and underlying assumptions

Historically wave models have been dealt with by means of different theories each having certain specific assumptions. It started with the linear wave theory developed by Airy (1895) which considered a simple sinusoidal wave travelling in space and varying with time. It also assumes potential theory for the calculation of the velocity field i.e. no friction losses and linearize the free surface boundary conditions and the differential equation itself [3].

This first approximation is valid for infinite depths, that is, when the wave is unaffected by the presence of the bottom $-d/L > 0.5$ and for cases when the steepness $e = H/L$, is sufficiently small and the linearization is acceptable i.e. very smooth waveforms. Those are the reasons why this first theory is called the linear theory or the small amplitude theory.

From here, other theories will take into account some of the non linearities by including a series approximation of the free surface in terms of the steepness $\eta = f(e)$, in order to consider the non linearities due to the surface kinematic and dynamic boundary conditions, allowing to model steeper waves. Other sources of non linearities like breaking waves or velocity skewness and asymmetries, are not accounted for in most theories and none of them considers friction losses. The term nonlinear is a complex concept that includes a whole spectrum of behavior that differ from the linear theory, but none of the wave theories captures those fully.

2.1. Assumptions, basic equations and boundary conditions

There are some common assumptions included the linear wave theory that strongly influences its accuracy and applicability. The main assumption of incompressibility is very convenient when dealing with water, and no drawbacks can be pointed out here. This assumption will lead to a very compact equation for the velocity [4]:

$$\nabla \cdot \vec{U} = 0 \tag{2-1}$$

Another assumption is the existence of a potential function f – associated to a conservative scalar field such as the gravitational field – that governs the velocity relies on the irrotationality:

$$\vec{\omega} = \nabla \times \vec{U} = 0 \tag{2-2}$$

Furthermore, the potential theory provides an elegant relation to obtain the velocities from the potential function ϕ :

$$\vec{U} = \frac{\partial \phi}{\partial x} \cdot \vec{i} + \frac{\partial \phi}{\partial y} \cdot \vec{j} + \frac{\partial \phi}{\partial z} \cdot \vec{k} \quad (2-3)$$

Both equations 2-1 and 2-3 combined together lead to the Laplace equation [4], known to be a linear differential operator, which is very convenient:

$$\nabla^2 \phi = 0 \quad (2-4)$$

The main drawbacks of the potential theory are related to i) neglecting the friction losses, which can be relevant for long domains and shallow waters and/or for breaking conditions, and ii) the implied irrotationality, which keeps the model from modelling rotating flows, like eddies or swirls. This, though, is quite assumable condition in waves if they are non-breaking that is why all relevant theoretical studies in wave hydrodynamics are formulated by means of irrotational flow. One of the consequences of irrotationality is that the waves are symmetrical about the wave crest. In steep waves, though, where the wave is close to breaking, this assumption is on its limit and the theory needs some adjustments to account for the inaccuracies arisen from some rotationality.

The boundary conditions for the potential theory can be classified as linear and nonlinear:

1. Linear boundary conditions: Linear boundary conditions are those having just linear differential operators in their definitions, for instance, a Dirichlet boundary condition for the velocity, such as normal velocity to a wall $v_n = 0$, this, in terms of potential variable, leads to:

$$\frac{\partial \phi}{\partial n} = 0 \quad (2-5)$$

2. Nonlinear boundary conditions: These are defined in terms of nonlinear differential operators or coupled variables– i.e. a definition of the boundary condition that is referring to the solution $\eta(x,t)$. Nonlinear boundary conditions can be kinematic or dynamic.

The kinematic boundary condition states that the flow cannot trespass certain boundaries or walls, which in a flat bottom leads to equation 2-5, but when dealing with the moving and irregular free surface, and the material derivative concept is used – DF/Dt along a moving particle – the expression obtained is:

$$\frac{\partial \phi}{\partial y} = \frac{\partial \eta}{\partial t} + u \frac{\partial \eta}{\partial x} + v \frac{\partial \eta}{\partial z}, \quad y = \eta(x, z, t) \quad (2-6)$$

which is highly nonlinear since it refers to the solution $\eta(x,z,t)$.

The dynamic boundary condition states that the pressure at the free surface is the same as the atmospheric, i.e. the atmospheric pressure outside the fluid is constant.

$$\rho \frac{\partial \phi}{\partial t} + .5\rho \left[\left(\frac{\partial \phi}{\partial x} \right)^2 + \left(\frac{\partial \phi}{\partial y} \right)^2 + \left(\frac{\partial \phi}{\partial z} \right)^2 \right] + \rho g \eta = f(t), \quad y = \eta(x, z, t) \quad (2-7)$$

Therefore, both the dynamic and kinematic boundary condition are sources of non linearities in the problem. Note the mixed terms in both expressions where the potential ϕ is together with the free surface elevation η , being both coupled unknowns.

2.2. Airy's linear theory

The linear theory implies a full linearization of the dynamic and kinematic boundary conditions [5].

$$\nabla^2 \phi = 0 \quad (2-8)$$

$$\frac{\partial \eta}{\partial t} = \frac{\partial \phi}{\partial y}, \quad y = 0 \quad (2-9)$$

$$\frac{\partial \phi}{\partial t} = -g\eta, \quad y = 0 \quad (2-10)$$

$$\frac{\partial \phi}{\partial y} = 0, \quad y = -d \quad (2-11)$$

The Airy wave has the following form:

$$\eta = \frac{H}{2} \cos(k \cdot x - \omega \cdot t + \theta) \quad (2-12)$$

where H is the wave height, $k = \frac{2\pi}{L}$ is the wave number, ω is the angular frequency, x is the spatial variable in one dimension, t is the time variable and θ is initial phase angle. This wave is fully linear and symmetric from the still water level.

The potential function can be derived using above equations as

$$\phi = \frac{H}{2} \cdot \frac{g}{\omega} \cdot \frac{\cosh(k(d+y))}{\cosh(kd)} (\mathbf{k} \cdot \mathbf{x} - \omega \cdot t) \quad (2-13)$$

From this expression, the other relevant parameters such as velocities and accelerations can be derived.

2.3. Stokes nonlinear wave theory

A generalization of the linear theory is made in the higher order theories. As it has been already mentioned, there are different theories depending on the approach to solve equation 2-4 and the kinetic and dynamic boundary conditions [3].

A step forward from the Airy wave is that of the Stokes higher order waves. Higher order Stokes theory is basically a generalization of the linear theory by including n harmonics when defining the free surface η :

$$\eta = \sum_{i=1}^n n_i = \sum_{i=1}^n A_i \cdot \varepsilon^{n-1} \cos(i(k \cdot x - \omega \cdot t)) + \theta(\varepsilon^n) \quad (2-14)$$

where n is the order of the Stokes wave and $\theta(\varepsilon^n)$ is a truncation error of order (ε^n).

Each of the components of the Stokes wave η_i has double the frequency from the one with lower order, and their amplitudes A_i can be obtained by applying the kinematic and dynamic boundary conditions expressing the nonlinear contributions by the Taylor expansion series of order n – the Stokes expansion.

Stokes waves break with the horizontal symmetry of the wave form in respect to the still water level, creating higher crests and shallower troughs as can be observed in Figure 2-1. This produces steeper crests and more impact-like forces than linear waves.

In addition to the Stokes's theory, there are several other nonlinear wave theories such as Cnoidal wave theory, Stream function theory and others. However, these theories are not discussed in this thesis.

2.4. Validity regions of various wave theories

It is important to understand which of the various wave theories need to be applied to a particular problem, where the wave characteristics and water depth are specified. The validity of various

wave theories must be known. This validation is composed of two parts namely mathematical validation and the physical validation.

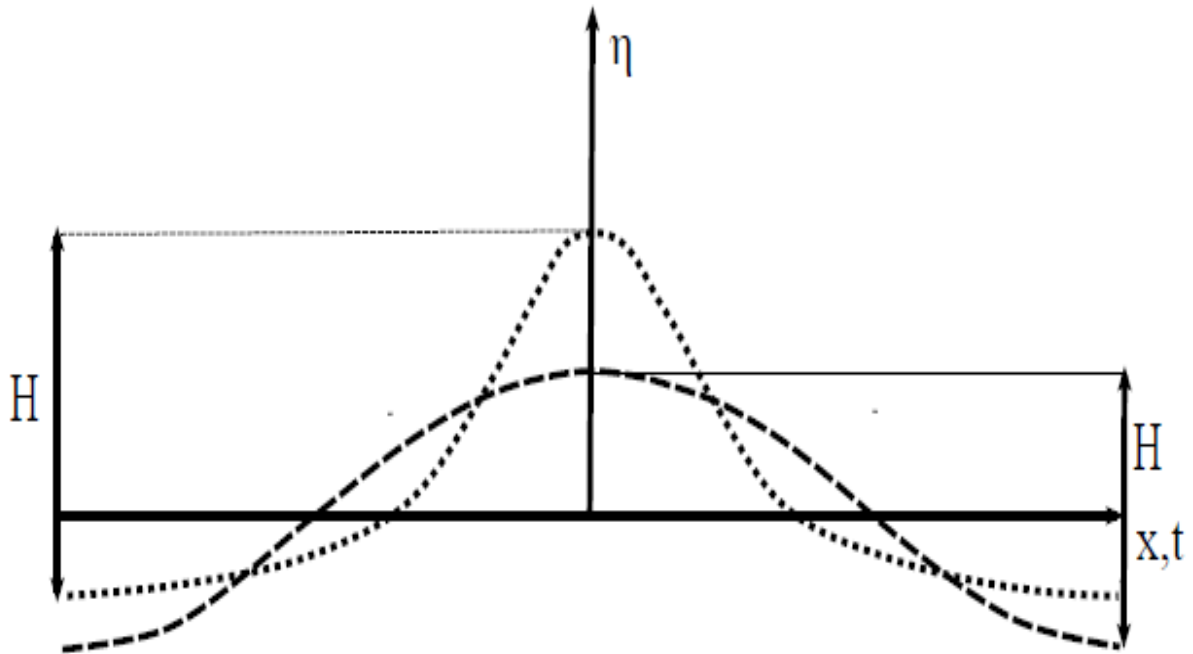


Figure 2-1 Qualitative representation of a linear wave form (dashed) vs Stokes wave (dotted)

The mathematical validation is the ability of a given wave theory to satisfy the mathematically posed boundary value problem. It is seen that while most of the wave theories satisfy the bottom boundary condition exactly, some wave theories only approximately satisfy the Laplace equation within the fluid. It is also seen that while all the theories satisfy the dynamic free surface boundary approximately, the kinematic free surface boundary condition is satisfied by the stream function theory [6].

The physical validity refers to how well the prediction of the various theories agrees with actual measurements. This part of the validation is generally difficult to obtain due to the problems of water wave tank design and measurement requirements [7].

The analytical validity of many wave theories has been examined by many researchers including [8]. Figure 2-2 shows the results of the comparison of the theories, denoting the regions for which each theory provides the best fit to the dynamic free surface boundary condition.

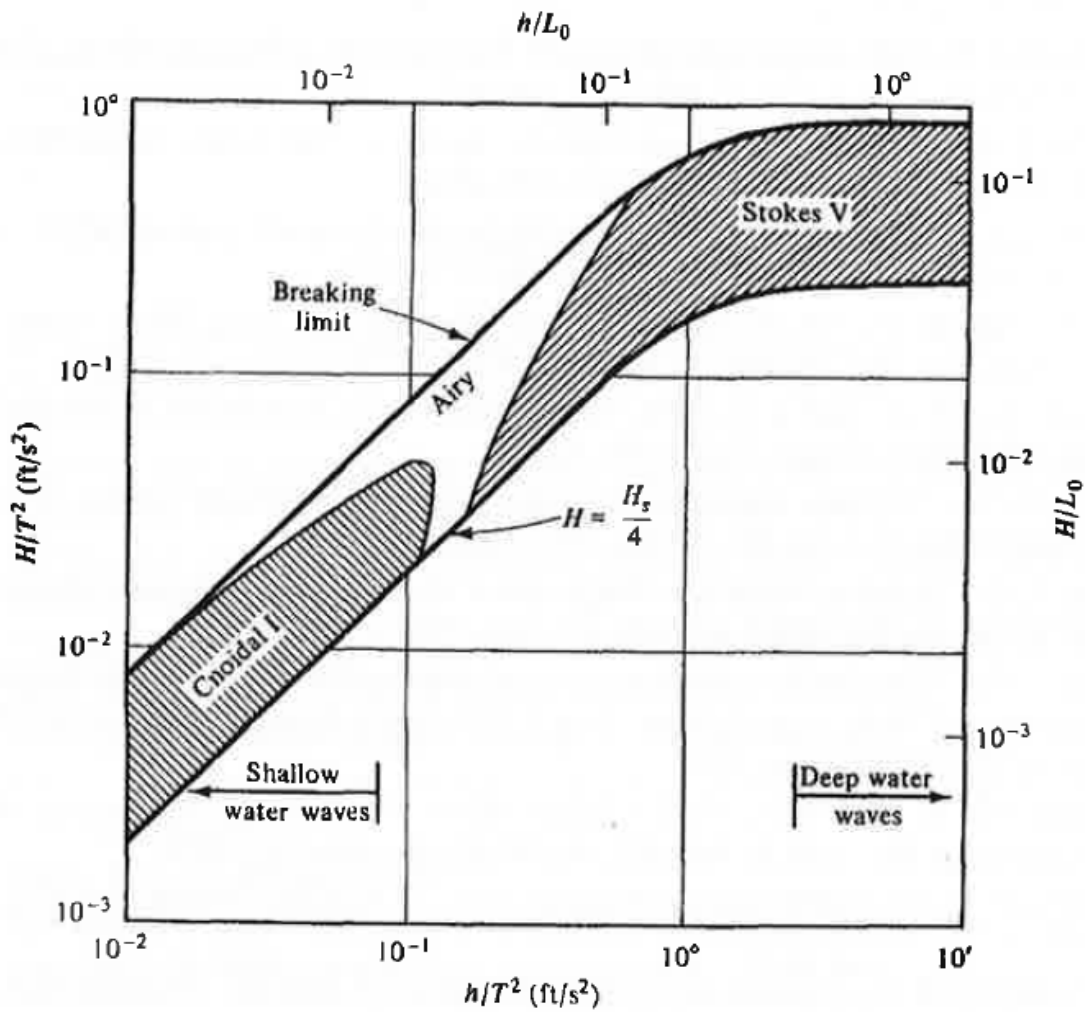


Figure 2-2 Validity range of various wave theories

As, it can be seen, the cnoidal wave theory does well in shallow water, while in deep water, the Stokes 5th order wave theory proves to be more applicable. It is also noted that the linear wave theory does well for intermediate water depths. However, as per literature, when high order stream function wave theory is used, it provides the best fit of all the theories including the shallow waters [6].

3. FEM modelling and analysis

3.1. General

The Jacket have been designed by using detailed elevations and plans provided from Total. The Topside is massive and are set to have a maximum operational weight of 28000 tons. Basic sketches have been provided by Total and have been modeled in different manners based on the individual load cases.

The program used to analyze and do the design is the structural engineering program called SAP2000 (Structural Analysis Program). The manual calculations have been done in Matlab and excel. The origin of the coordinate system is set to the south-west corner of the highest Jacket plan located at $z = 22m$ for the x and y coordinates and at mean sea level for the z-coordinate. The modeling of beams and columns in SAP2000 are done from the centroid of the assigned sections/profiles.

3.2. SAP2000

SAP2000 is a powerful analysis & design program that was introduced for over 30 years ago by CSI (Computers and Structures INC). SAP2000 can be used to handle simple 2D exercises too complex 3D structures. The goal when making the program was too simplify the engineer's calculation process in form of modeling, design and optimization with help from a powerful analysis "engine" and a versatile user interface [9].

SAP2000 is known for its flexibility between international borders, multiple sets of standards, sectional dimensions and material qualities can be used.

The program can also perform different loading analysis such as: static linear/nonlinear analysis, buckling analysis, influence lines analysis, pdelta analysis, accidental load analysis and vibration analysis. All the capacity checks are based on the given standard and the program compares the acting analysis forces to the sectional capacities [10]

3.3. Design parameters

The information following was provided by total and the approximations used for SAP2000 have the following assumptions:

- 100 year return period for both wave/current.
- Maximum individual wave height for all directions.
- The largest current velocity for any given directions.

3.3.1. Waves

The extreme design wave to be used in the analysis is defined by maximum wave height associated with average time period. The values for different return period is shown in Table 3-1. It is noted that 100 year return period wave is used for SLS and ULS analysis. H_{max} is maximum individual wave height, T_p is peak wave period for H_{max} , Cr_{max} is maximum wave-crest-elevation relative to MSL, H_s is significant wave-height (3 hours).

Table 3-1 Wave parameters

Return Period (years)	H_{max}	T_p	Cr_{max}	H_s
1	19.8	13.2	12.4	10.3
10	24.5	14.7	15.3	12.6
100	28.8	15.9	18.1	14.8
10 000	37.0	17.9	23.4	18.8

3.3.2. Current

The surface current for 100 year are given in Table 3-2. Generation of the vertical current profile based upon the surface current is given in Table 3-3. Current blockage factor is in accordance with NORSOK N-003 [11]. The blockage factor is taken as 0.85 for Jacket with more than 3 legs.

Table 3-2 Surface current for 100 year return period

Analysis angle	Geographical Direction	Return period 100 year [m/s]
0	West	0.78
45	South West	1.03
90	South	1.08
135	South East	1.02
180	East	1.05

Table 3-3 Vertical current profile for 100 year return period

Distance from mudline up to water surface [m]	Current profile [Ratio of surface current speed]
0.0	0.65
7.0	0.68
39.0	0.69
64.0	0.69
74.0	0.68
84.0	0.71
94.0	0.77
105.0	0.88
114.0	1.00

3.4. Modal Analysis

3.4.1. Eigenvector analysis

Eigenvector analysis determines the undamped free-vibration mode shapes and frequencies of the system. These natural modes provide an excellent insight into the behavior of the structure. They can also be used as the basis for response- spectrum or time-history analyses [12]

SAP2000 uses the following formula to solve for generalized eigenvalue problems [10]:

$$[K - \Omega^2 M] \phi = 0 \quad (3-1)$$

Where K is the stiffness matrix, Ω and M are diagonal matrices which represents eigenvalues and mass. ϕ is the corresponding eigenvectors (mode shapes).

For a system with forced damping the equation of motion becomes [13]:

$$F(t) = M \cdot x'' + C \cdot x' + K \cdot x \quad (3-2)$$

For a system with free undamped vibration the equation of motion becomes:

$$M \cdot x'' + K \cdot x = 0 \quad (3-3)$$

The system will in this case not have an external force applied as it vibrates, although it will need at least one initial conditions such as a initial force or a displacement in order to start vibrating.

As specified in the introduction of this section SAP2000 works with an undamped free-vibration system so equation 3-3 becomes relevant. The following assumptions is made for such a system:

No damping in the system.

No external forces as the system is moving.

For an undamped free vibrational system with harmonic motion at the same frequency (ω) and phase angle (θ), the deflection can be written as [12].

$$x(t) = \phi \cdot \cos(\omega t - \theta) \quad (3-4)$$

The derivations of the displacements based on t becomes:

$$x'(t) = -\omega \cdot \phi \cdot \sin(\omega t - \theta) \quad (3-5)$$

$$x''(t) = -\omega^2 \cdot \phi \cdot \cos(\omega t - \theta) \quad (3-6)$$

Next step will be to input equation 3-5 and 3-6 into equation 3-3:

$$0 = M \cdot (-\omega^2 \cdot \phi \cdot \cos(\omega t - \theta)) + K \cdot (\phi \cdot \cos(\omega t - \theta)) \quad (3-7)$$

$$0 = (-\omega^2 \cdot M + K) \cdot \phi \cdot \cos(\omega t - \theta) \quad (3-8)$$

In order for equation 3-8 to be true one of the contributions needs to be zero and as $\cos(\omega t - \theta)$ can only be zero for some cases:

$$\cos(\omega t - \theta) = n \cdot \pi = 0, \text{ where } n = 1,2,3 \dots$$

Thus, the other contribution needs to be zero and the equation becomes is the same formula as SAP2000 in equation 3-1:

$$0 = (-\omega^2 \cdot M + K) \cdot \phi \quad (3-9)$$

Because equation 3-9 is based on matrices, we need to find a value that corresponds to be zero. To find the value of a matrix we need to base it on the determinant of matrices M and K which converts the matrix into a value.

$$|-\omega^2 \cdot M + K| = 0 \quad (3-10)$$

For a 2D beam element, the stiffness element matrix and the mass matrix may be defined as shown in equation 3-11 [14].

$$[K] = \frac{EI}{L^3} \begin{bmatrix} 12 & 6L & -12 & 6L \\ 6L & 4L^2 & -6L & 2L^2 \\ -12 & -6L & 12 & -6L \\ 6L & 2L^2 & -6L & 4L^2 \end{bmatrix} \quad [M] = \frac{\rho AL}{420} \begin{bmatrix} 156 & 22L & 54 & -13L \\ 22L & 4L^2 & 13L & -3L^2 \\ 54 & 13L & 156 & -22L \\ -13L & -3L^2 & -22L & 4L^2 \end{bmatrix} \quad (3-11)$$

The above equations can be written for each 2 node element and combined together to form global mass and stiffness matrices, M and K respectively. The natural frequencies can be obtained using these matrices and equation 3-10

3.5. ULS and SLS analysis

3.5.1. Ultimate limit state (ULS)

This limit state takes into account that all foreseen loads can be resisted with sufficient margin. ULS is also varying the material factor depending on which of the load cases that are governing. The load cases are divided into two groups where either a) permanent or variable actions are governing or b) the environmental actions are governing.

3.5.2. Serviceability limit state (SLS)

SLS is to make sure that the deformation does not interrupt the functionality of normal operations of the structure. Normally the requirements for serviceability is chosen by the operator. Usually the material factor is set to 1 for all load actions acting on the structure.

The limit states are shown in Table 3-4 according to NORSOK N-001 [15]:

Table 3-4 Limit states and corresponding factors

Limit state	Action combinations	Permanent actions	Variable actions	Environmental actions
ULS	A	1.3	1.3	0.7
ULS	B	1.0	1.0	1.3
SLS		1.0	1.0	1.0

4. Case study part 1: Effect of wave theory on analysis

Environmental loading plays an important role when it comes to offshore structures. These include wave loading along with wind and the current. Various wave theories are available in the literature and it is interesting to see the effect of various wave theories on the structural response of the structure. To investigate this, a study is first performed on a simple beam. Linear Airy's wave theory is applied and results are compared with manual calculations. This is done in order to both understand the wave theories as well as to verify the FE software results with manual calculations at-least for the linear wave theory. In the end, these wave theories are applied to the complex big Jacket and results are compared.

4.1. Analysis on a simple column

The following sub-sections are based on comparing results found from wave loading in SAP2000 against manual calculations. The purpose of this is to get a confidence that the applied wave loading in SAP2000 for the Martin Linge Jacket are used correctly. The example consists of a single tubular cantilever column and has an applied wave load acting at zero degrees on the column. Also, the current and wind load is neglected for this study. The section and material properties of the column is shown in Table 4-1.

Table 4-1 Section and material properties of column

Section property	Value
Length	150m
Diameter	1.5m
Material	S355

4.1.1. Analysis in SAP2000 using linear Airy's wave theory

The member is modelled in the FE software and linear wave theory is used to generate the particle velocities and accelerations. A wave height of 28.8m and wave period of 15.5 seconds is considered. The wave profile and horizontal wave particle velocities along a section of the length of the member is generated in SAP2000 and shown in Figure 4-1. The drag and inertia coefficients are taken as per API by the software. These are shown in Table 4-2.

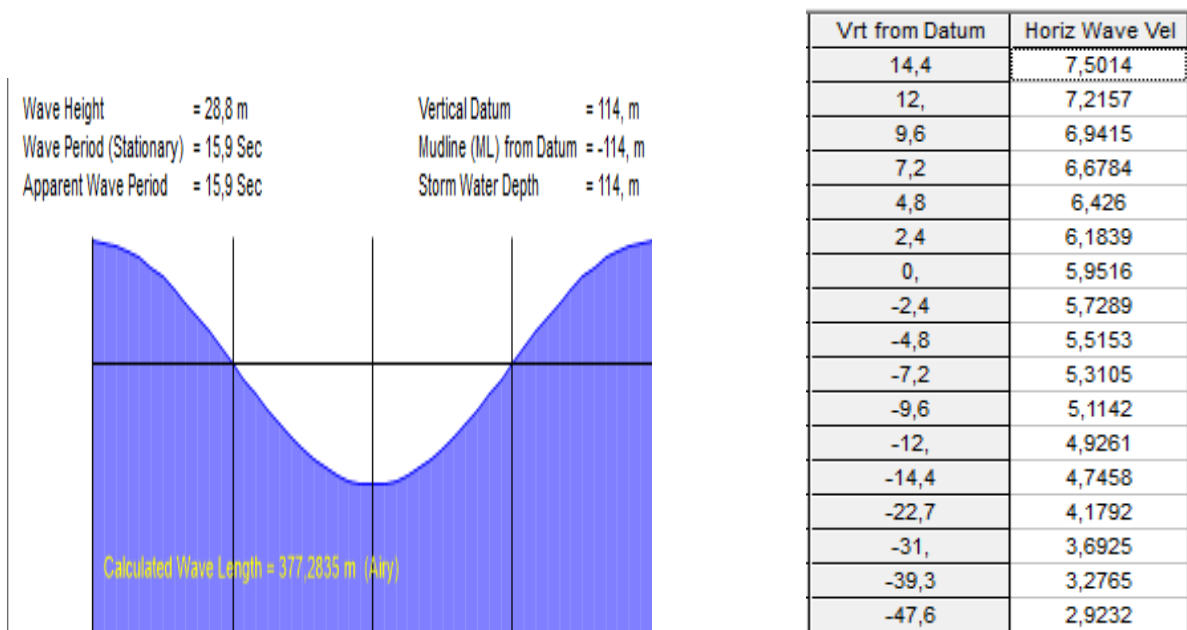


Figure 4-1 Wave profile and horizontal particle velocity from SAP2000

Table 4-2 Drag and inertia coefficients are taken as per API

Location	Drag coefficient	Inertia Coefficient
Above High Tide Elevation	0.65	1.6
Below or at High tide Elevation	1.05	1.2

The wave loads on the member is derived using the morison's equation and loading is generated automatically on the member as shown in Figure. The total wave load acting on the member is found out from the base reaction for the wave load case. The total wave load is 1291.45 kN.

4.1.2. Manual calculations using linear wave Theory

It is intended to check the above obtained wave particle velocity as well as wave loading from the FE software with manual calculations. This is done to gain deeper understanding of the wave theories. For this study, only the linear Airy theory is considered and results are compared with those obtained from SAP2000.

Natural frequency:

$$\omega = \frac{2\pi}{T_p}; \quad \omega = 0.3952 \text{ rad/s}$$

Estimation using iteration process

Table 4-3 Water depth relation with frequency

Water depth	ω^2 value
Intermediate water	$g \cdot k \cdot \tanh(kd)$
Deep water	$g \cdot k$

The natural frequency of the wave is dependent on the wave number for intermediate water in two separate occasions in one equation. An iteration process [4] is used to find k for intermediate water based on dispersion relation from deep water. It is possible to find an estimate to the wave number factor for intermediate water when initial deep water wave number is equal to intermediate water:

$$\frac{\omega^2}{g} = k_{dw} = k_{new} \cdot \tanh(k_{new} \cdot d)$$

$$k_{dw} = 0,015918293 \frac{rad}{s^2}$$

Table 4-4 Iteration for calculation for k

New guess of wave number	$k * \tanh(kd)$
0.01661	0.015873861
0.01662	0.015885058
0.01663	0.015896254
0.01664	0.015907448
<u>0.01665</u>	<u>0.01591864</u>
0.01666	0.015929831

From the Table 4-4 it shows that when k=0,01665 we get approximately the same value as for k_{dw}=0,015918293, thus we will use the given wave number k=0,01665 for intermediate water to calculate horizontal velocity.

Horizontal wave velocity in intermediate water:

$$u = \frac{\eta_0 \cdot k \cdot g}{\omega} \cdot \frac{\cosh k(z + d)}{\cosh(kd)} \cdot \sin(\omega t - kx)$$

In the worst case scenario, the velocity need to be at its largest.

Therefore,

$$\sin(\omega t - kx) = 1$$

At SWL, $z = 0m$:

$$u(z = 0) = \frac{14,4 \cdot 0,01665 \cdot 9,81}{0,3952} \cdot \frac{\cosh 0,01665(0 + 114)}{\cosh(0,01665 \cdot 114)}$$

$$u(z = 0) = 5,952 \frac{m}{s}$$

For specified depths (z):

Table 4-5 Calculation of horizontal particle velocity

Elevation (z)	Horizontal velocity (m/s)
14.4	7.501374191
0	5.952000971
-14.4	4.746419859
-28.8	3.814995572
-43.2	3.103928335
-57.6	2.572146362
-71.8	2.193347753
-86.2	1.934930648
-100.6	1.788276612
-114	1.744672958

Wave length, intermediate water:

$$L = \frac{g \cdot T_p^2}{2\pi} \cdot \tanh(kd); \quad L = \frac{9,81 \cdot 15,9}{2\pi} \cdot \tanh(0,01665 \cdot 114); \quad L = 377,38m;$$

Keulegan-Carpenter Number:

$$N_{KC} = \frac{u_{max} \cdot T_p}{D}; \quad N_{KC} = \frac{7,501374191 \frac{m}{s} \cdot 15,9s}{1,5m}; \quad N_{KC} = 79,52;$$

We have a drag dominant force acting if $N_{KC} > 30$, meaning we can neglect the inertia force [4].

Drag force per unit length

It is assumed that the members under the wave crest are rough members and members above wave crest are smooth members giving drag coefficient as $C_D = 1,05$ for members below high tide elevation and $C_D = 0,65$ for members above hightide elevation.

$$f_D(z, t) = \frac{1}{2} \rho \cdot C_D \cdot D \cdot u(z, t) \cdot |u(z, t)|$$

Wave force without interaction from current and wind

$$F_{tot} = F_D = \int_0^{wave\ crest} f_{D,smooth}(z) dz + \int_{-d}^0 f_{D,rough}(z) dz$$

$$F_D = \int_0^{14,4} \frac{1}{2} \cdot 1025 \cdot 0,65 \cdot 1,5 \cdot \left(\frac{14,4 \cdot 0,01665 \cdot 9,81}{0,39516889} \cdot \frac{\cosh k(z+d)}{\cosh(0,01665 \cdot 114)} \cdot 1 \right)^2 dz$$

$$+ \int_{-114}^0 \frac{1}{2} \cdot 1025 \cdot 1,05 \cdot 1,5 \cdot \left(\frac{14,4 \cdot 0,01665 \cdot 9,81}{0,39516889} \cdot \frac{\cosh k(z+d)}{\cosh(0,01665 \cdot 114)} \cdot 1 \right)^2 dz$$

$$F_D = \int_{-114}^{14,4} 1521 \cdot (\cosh 0,01665 (z + 114))^2 dz + \int_{-114}^0 2457 \cdot \cosh 0,01665 (z + 114) dz$$

$$F_D = 1521 \cdot 212,972N + 2457 \cdot 391,153N$$

$$F_D = 1284,99kN$$

4.1.1. Comparison of SAP2000 and manual calculations

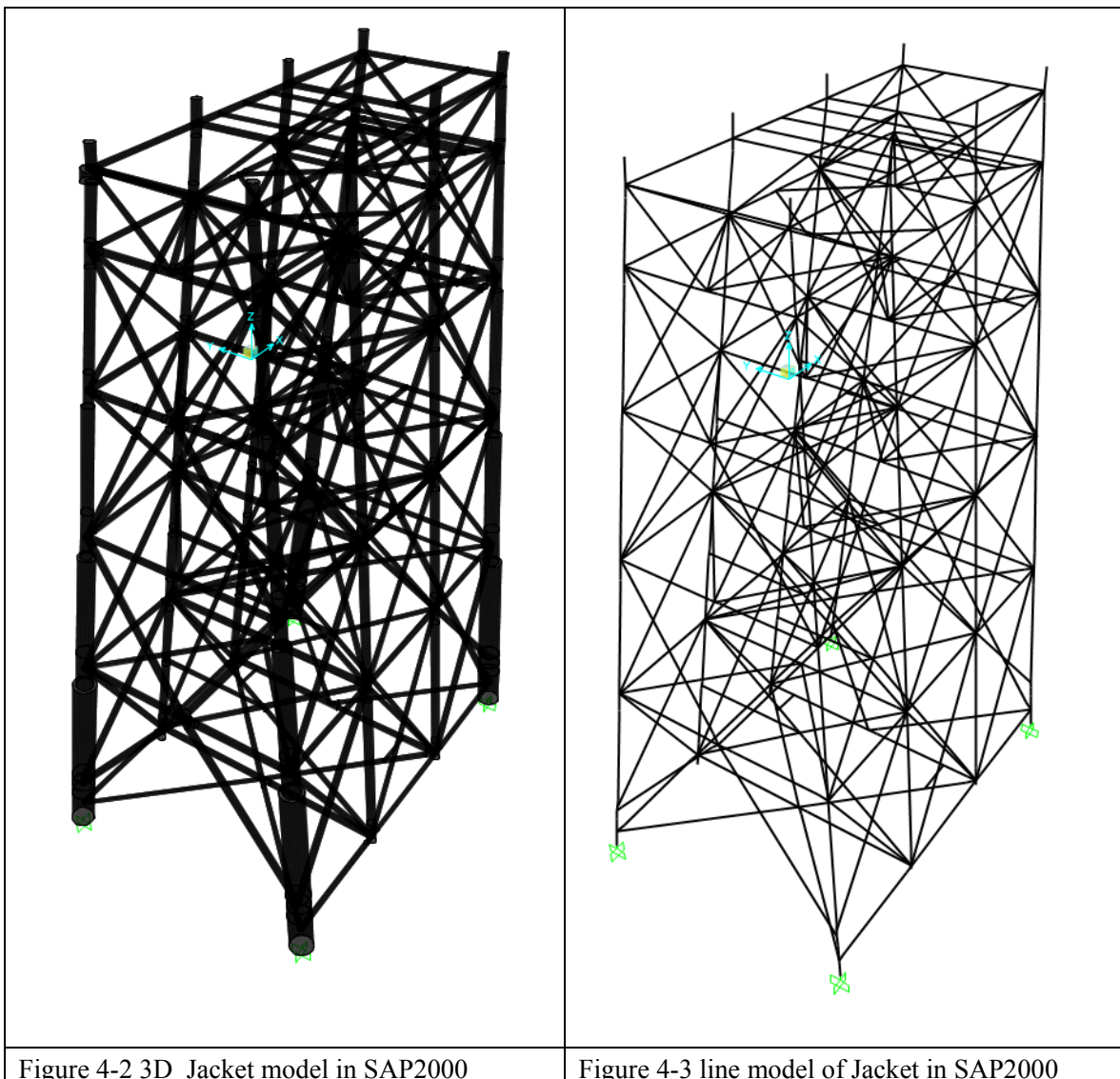
The results from the FE software SAP2000 are found to be in good agreement with the manual calculations for the linear wave theory. This study is now expanded further to the complex big Jacket structure with Topside on it. It is intended to observe the Jacket response under different wave theories and compare these results. Both linear Airy's wave theory and nonlinear 5th order Stoke's wave theory is used.

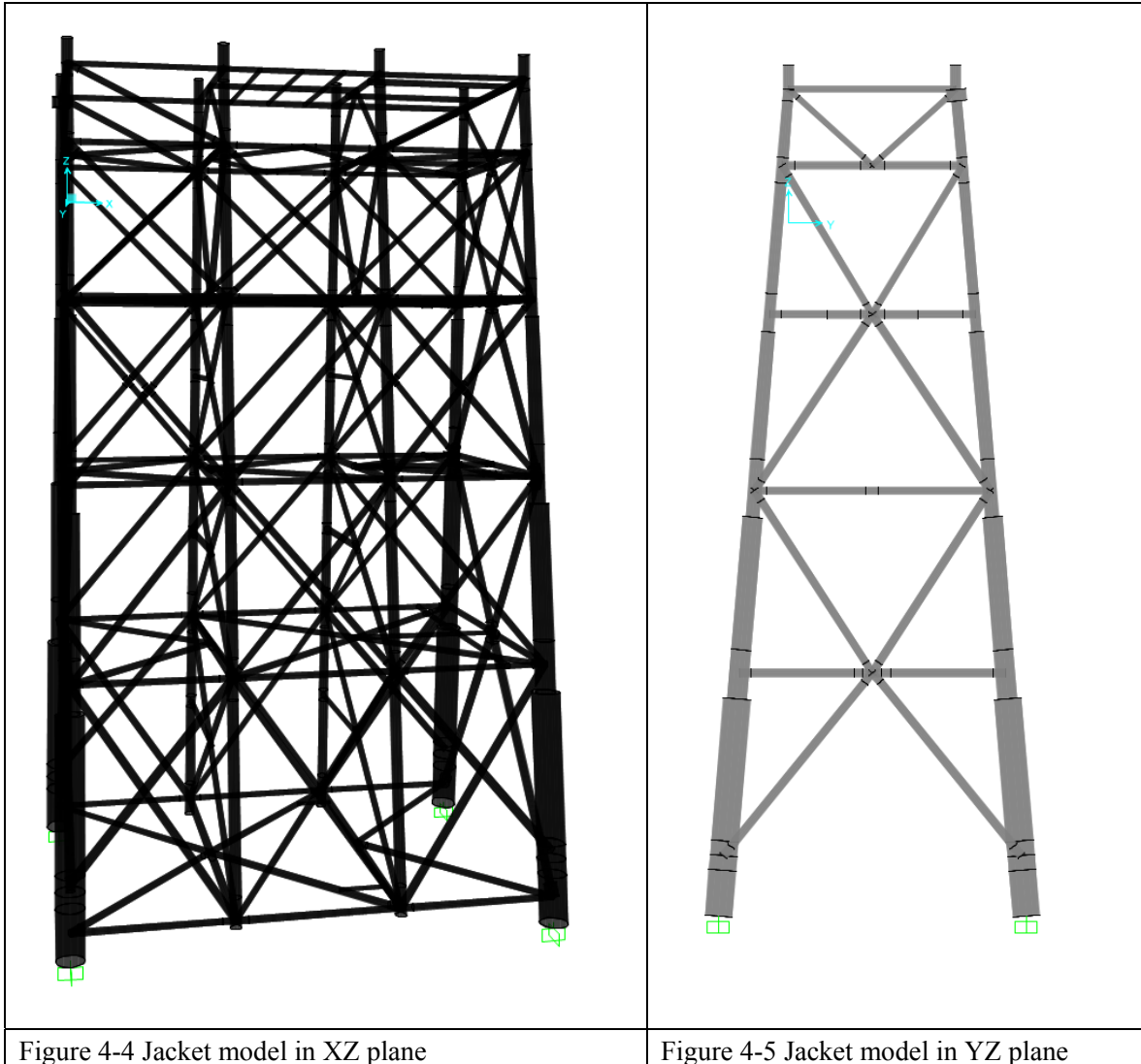
4.2. Analysis of complex Jacket structure

The understanding gained in the earlier part of this case study is extended further on a real offshore structure. The chosen structure is Martin Linge platform which is a fixed Jacket type platform with Topside on it. This is one of the heaviest platforms in the NCS region.

4.2.1. Structural model

The structural details of the Jacket were provided by Total and are used to make a complete Jacket model in SAP2000. The model is shown in Figure 4-2 to Figure 4-5.





It is noted that only limited information was made available for the Topside. This includes a rough estimate of Topside weight along with some sketches of the module dimensions. The module wise weight distribution and CoG locations are also not known. However, the Topsides information from a similar platform were available (referred here as platform x) and this information is use to make logical assumptions of the weight of the Martin Linge Topside modules. The weight of platform x is 24774 tons. The flare boom, cranes, live load areas and helideck are not included in the Topside model.

The Martin Linge Topside is divided into several deck levels and a weight factor of 1.13 is obtained for each module. The weight factor is obtained using the weight information of the platform x and comparing it with Martin Linge Topside weight as shown in Table 4-6.

$$\text{Weight factor} = \frac{28000\text{ton}}{24774,4\text{ton}} = 1,1302$$

$$\text{Martin Linge}_{\text{weight}} = \text{Weight factor} * \text{Weight of platform x modules}$$

Table 4-6 Weight comparison between platform x Topside and Martin Linge Topside

Levels	Platform x [ton]	Martin Linge_{weight} [ton]
Cellar deck	7400,8	8364,4
Modul deck	10979,6	12409,1
Modul 1 – 6	3937	4449,6
Living quarters	2457	2776,9
Total	24774,4	28000

From Table 4-6 a rough estimation of the Topside modules is obtained for Martin Linge. The dimensions of the modules is obtained using some of the sketches provided. These are shown in Figure 4-6 and Figure 4-7.

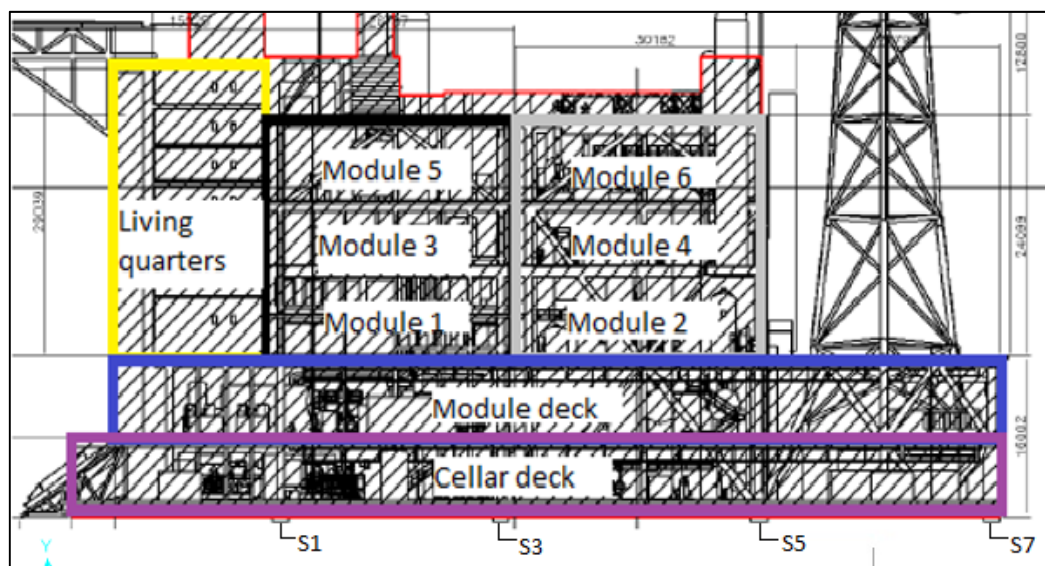


Figure 4-6 Topside drawing received from TOTAL

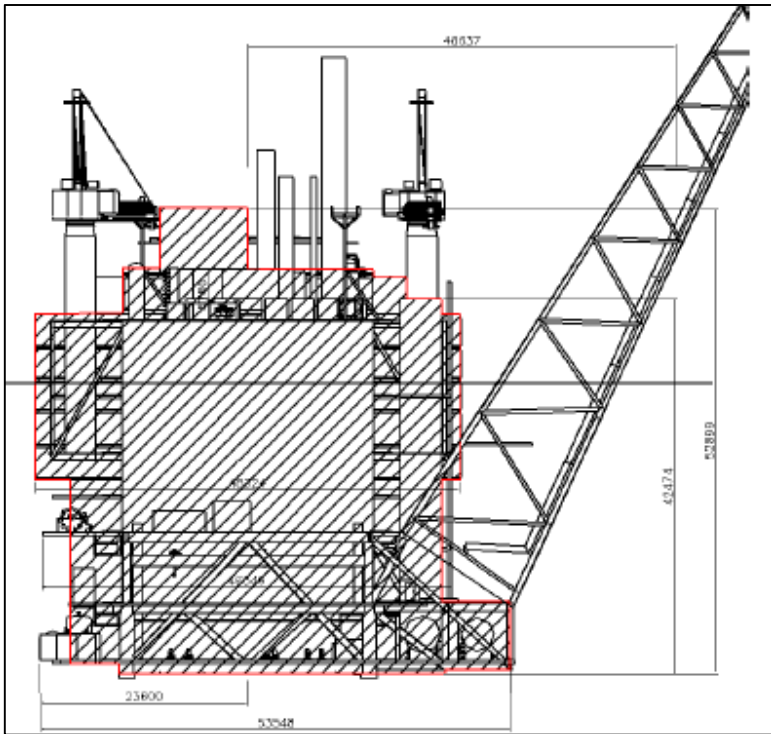


Figure 4-7 Topside drawing received from TOTAL

The modules are modelled in SAP2000 with corresponding weight and dimensions. These are shown in Figure 4-8. The entire platform model is shown in Figure 4-9.

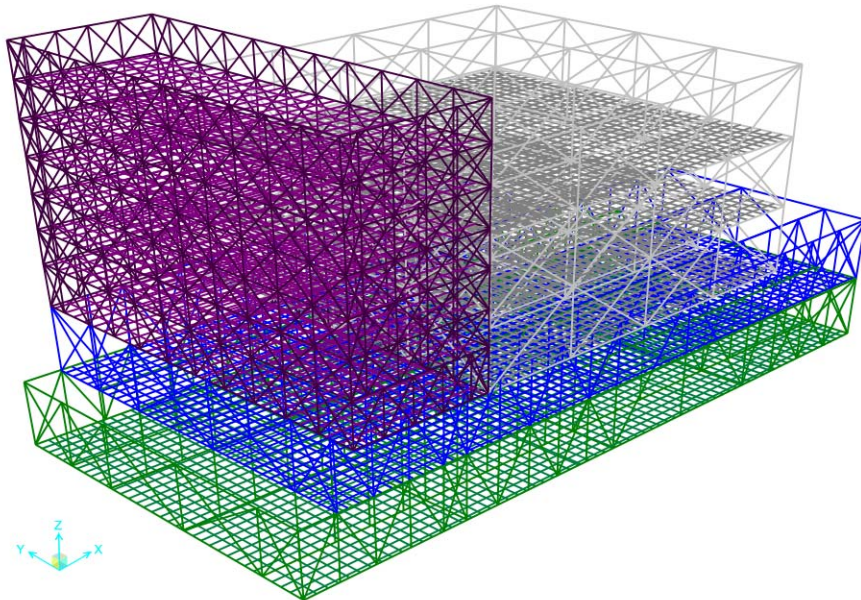


Figure 4-8 Topside model in SAP2000

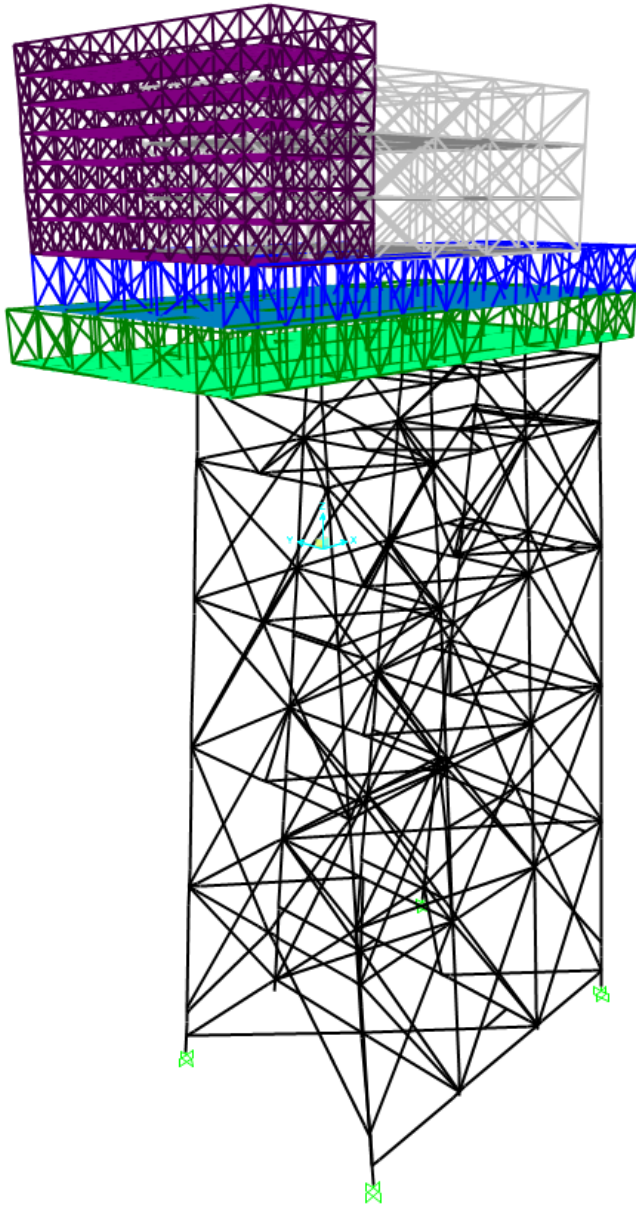


Figure 4-9 Topside and Jacket model in SAP2000

The Topside modules are developed using I-sections and S355 material having steel density of 7850 kg/m³. The target weight for each module is obtained by increasing the density of the sections. The density factor is obtained by dividing the target weight with model weight for each module and shown in Table 4-7.

$$\text{Density factor} = \frac{\text{Martin Linge module weight}}{\text{Model weight in SAP2000}}$$

Table 4-7 Density factor for various modules of Martin Linge Topside

Levels	Target weight [ton]	Model weight [ton]	Density factor	Density [$\frac{\text{ton}}{\text{m}^3}$]
Cellar deck	8364,4	5876	1,423	11,171
Modul deck	12409,1	3982	3,116	24,458
Modul 1 – 6	4449,6	1509	2,949	23,150
Living quarters	2776,9	2005	1,3846	10,868
Total	28000			

4.2.2. Structural analysis – Natural frequencies, SLS and ULS

Nonlinear static analysis as well as Eigenvalue analysis has been performed. The non-linearity considered are mainly the force nonlinearity (nonlinear wave loading). The free vibration natural frequencies and corresponding mode shapes are calculated from the Eigenvalue analysis. Code check for Jacket members is performed as per NORSOK-004 standard [16]. Analysis is also performed using linear Airy’s wave theory and results are compared with those obtained using non-linear Stokes 5th order wave theory.

4.2.3. Loading conditions – Load cases and combinations

The loading considered in the static analysis is the dead load, wave load and the current load. Dead load is permanent actions. It is the structural mass and include all fixed items on the decks and Jacket. Wave loads are the metocean actions. Wave loading is applied using both linear Airy’s wave theory as well as nonlinear Stokes 5th order theory and results are compared. The wave particle velocities and accelerations are calculated using these theories. Morison’s equation is used to calculate the wave load on Jacket members. The hydrodynamic drag and mass coefficients (C_d and C_m) are taken as per API code. The use of API code is due to software restrictions.

For SLS and ULS assessment, a 100 year return wave with a wave height of 28,8 meters and time period of 15,5 seconds is used. The wave load is defined in 5 directions at an angle of 0deg, 45deg, 90deg, 135deg and 180deg and corresponding load case is generated for each direction. The current is applied in the direction of wave in the respective load case. All the above defined load cases are combined as per the ultimate limit state (ULS) criteria given in standard code NORSOK N-001 [15]. The load combinations and load factors for ULS and SLS analysis are shown in Table 4-8 and Table 4-9.

Table 4-8 Load combinations considered in the ULS analysis

Load case	Permanent actions	Variable actions	Environmental actions	Direction wave	Direction current
ULS _{A1}	1.3	1.3	0.7	0 ⁰	0 ⁰
ULS _{A2}	1.3	1.3	0.7	45 ⁰	45 ⁰
ULS _{A3}	1.3	1.3	0.7	90 ⁰	90 ⁰
ULS _{A4}	1.3	1.3	0.7	135 ⁰	135 ⁰
ULS _{A5}	1.3	1.3	0.7	180 ⁰	180 ⁰
ULS _{B1}	1.0	1.0	1.3	0 ⁰	0 ⁰
ULS _{B2}	1.0	1.0	1.3	45 ⁰	45 ⁰
ULS _{B3}	1.0	1.0	1.3	90 ⁰	90 ⁰
ULS _{B4}	1.0	1.0	1.3	135 ⁰	135 ⁰
ULS _{B5}	1.0	1.0	1.3	180 ⁰	180 ⁰

Table 4-9 Load combinations considered in the SLS analysis

Load case	Permanent actions	Variable actions	Environmental actions	Direction wave	Direction current
SLS	1.0	1.0	1.0	0 ⁰	0 ⁰
SLS	1.0	1.0	1.0	45 ⁰	45 ⁰
SLS	1.0	1.0	1.0	90 ⁰	90 ⁰
SLS	1.0	1.0	1.0	135 ⁰	135 ⁰
SLS	1.0	1.0	1.0	180 ⁰	180 ⁰

4.2.4. Analysis results – Natural frequencies

The free vibration natural time period and vibration modes for the model are shown in Table 4-10. The first and second modes are sway modes in the two transverse directions. The third mode corresponds to the torsional vibration mode. It is to be noted that these modal parameters only depend on the mass and stiffness of the structure and are independent of the external loading. Therefore, for both the cases of linear and nonlinear wave theory, these values remains the same.

Table 4-10 Natural periods and vibration modes for the Jacket model

Modes	1 st	2 nd	3 rd
Time period	2.22	3.00	1.61
Vibration mode	Sway-X	Sway-Y	Torsion

4.2.5. Analysis results – Leg displacements (SLS)

The nonlinear static response of the Jacket is observed in terms of displacement of one of the main legs (leg A shown in Figure 4-10). Displacement of the leg along its height is obtained for various load combinations. The leg displacement U1 in x-direction is obtained using both linear and nonlinear wave theory and values are shown in Figure 4-11 and Figure 4-12. The comparison of the results is shown in Figure 4-13. The displacement U2 in y-direction obtained using linear and nonlinear wave theory is shown in Figure 4-14 and Figure 4-15 respectively. The comparison is shown in Figure 4-16.

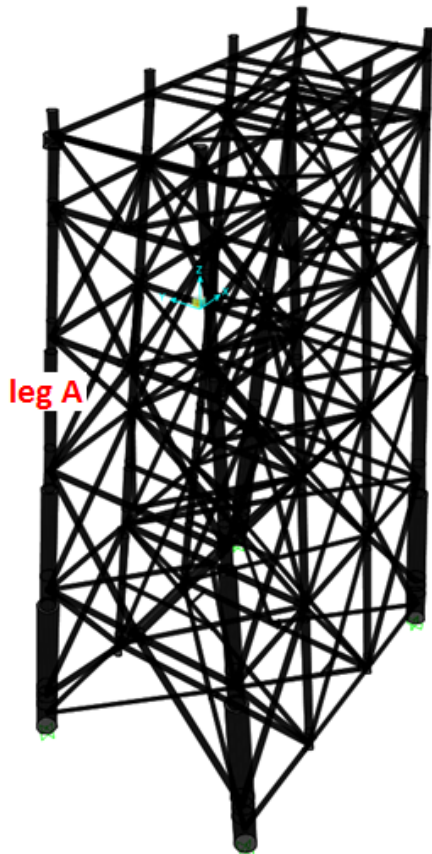


Figure 4-10 Considered leg A of the Jacket

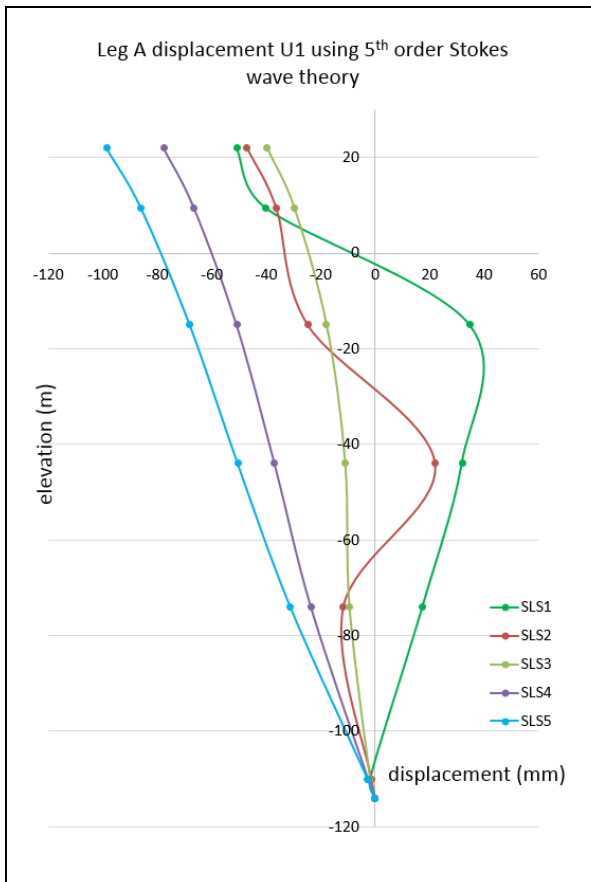


Figure 4-11 Leg A displacement U1 (x-direction) using nonlinear wave theory

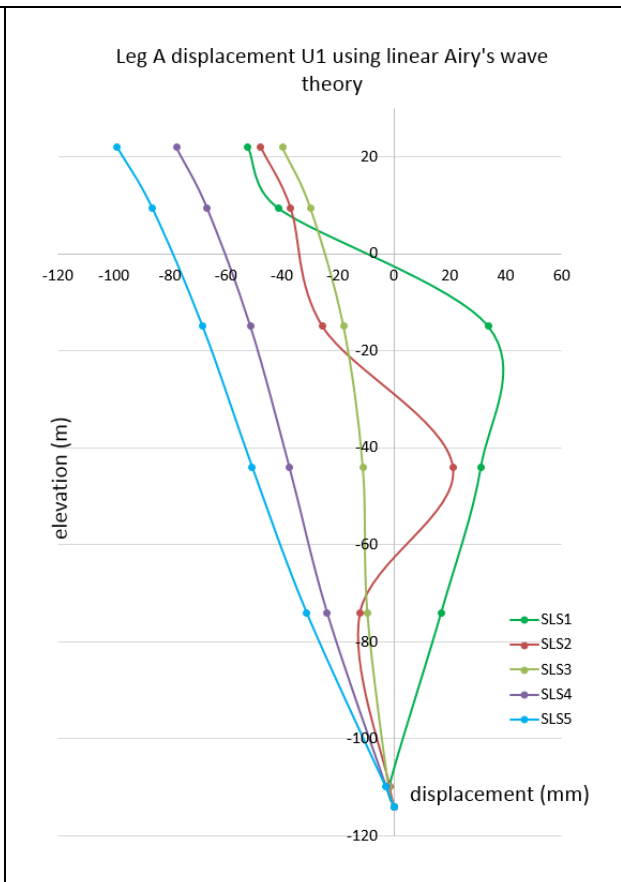


Figure 4-12 Leg A displacement U1 (x-direction) using linear Airy's wave theory

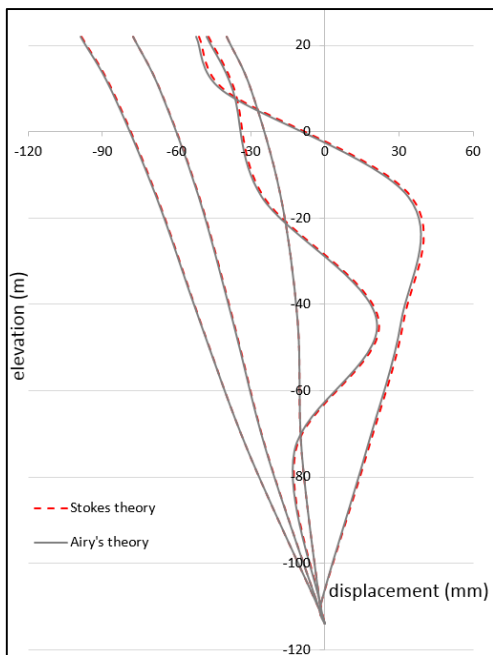


Figure 4-13 Leg A displacement U1 comparison between linear and nonlinear wave theory

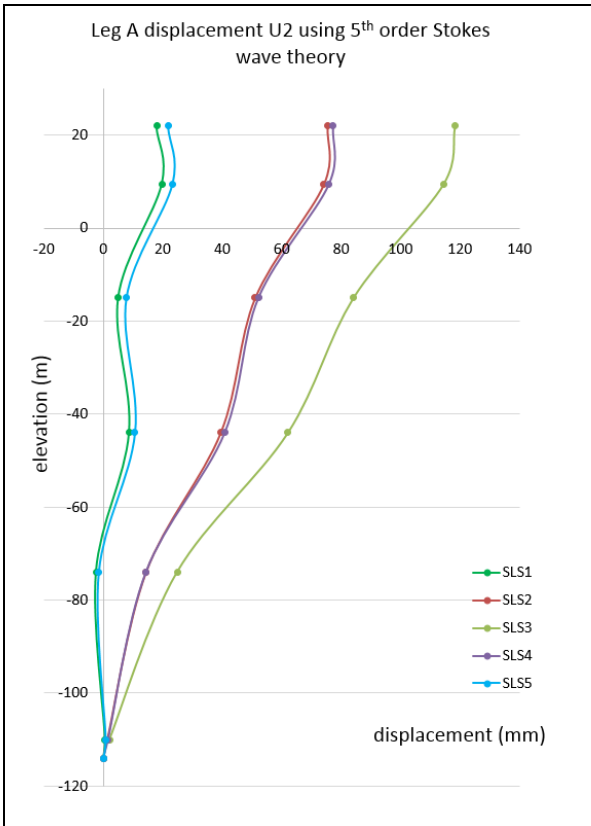


Figure 4-14 Leg A displacement U2 (y-direction) using nonlinear wave theory

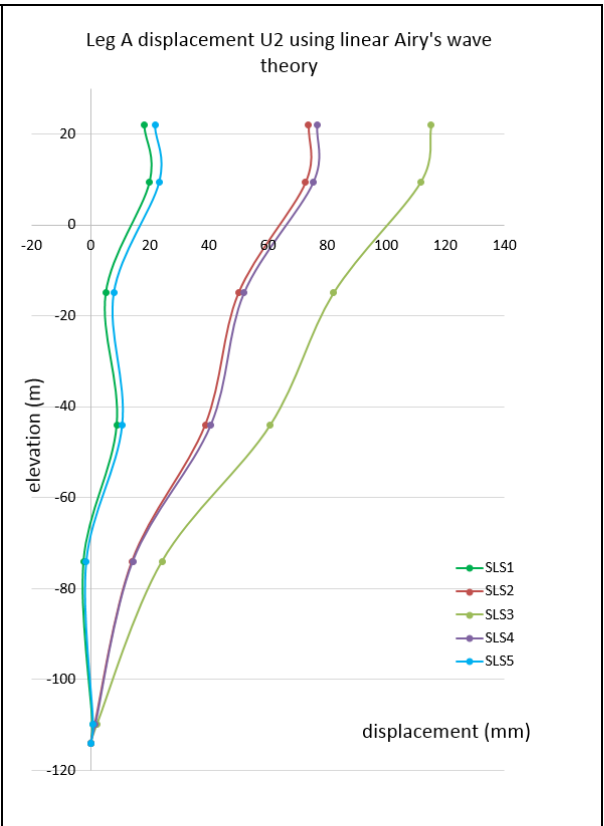


Figure 4-15 Leg A displacement U2 (y-direction) using linear Airy's wave theory

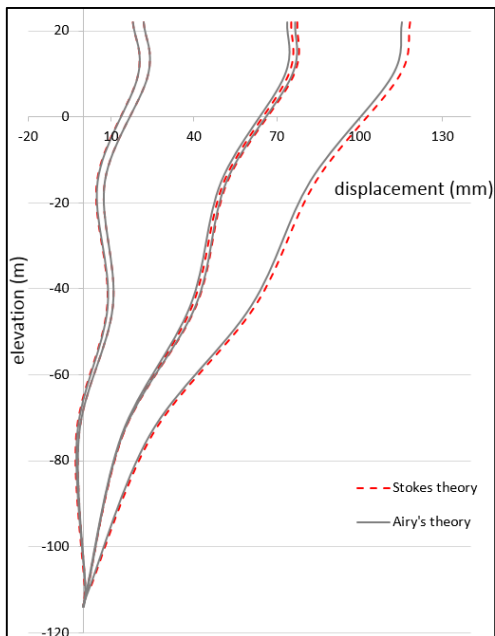


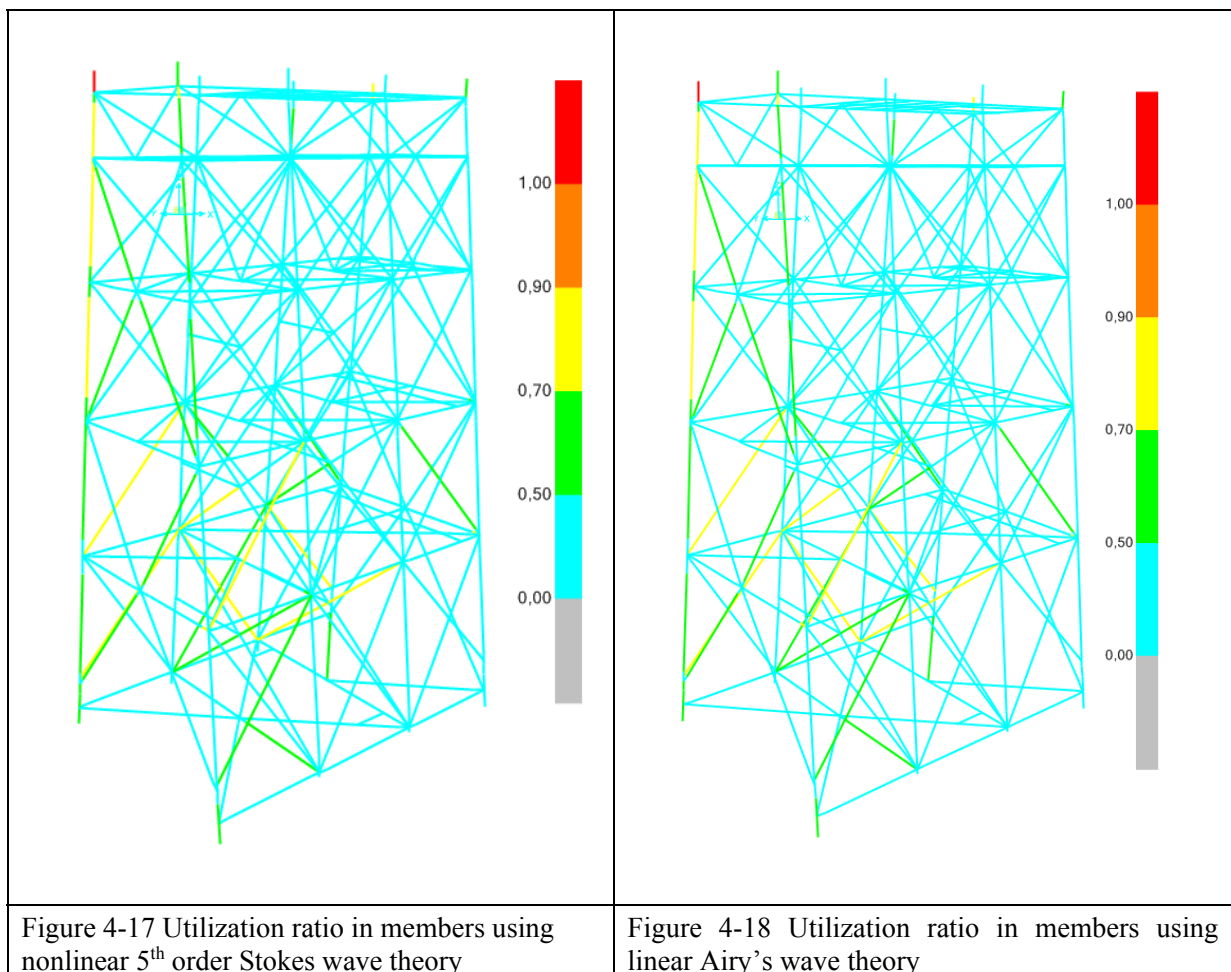
Figure 4-16 Leg A displacement U1 comparison between linear and nonlinear wave theory

4.2.6. Analysis results – Member capacity check (ULS)

Code check for Jacket members is performed as per NORSOK-004 standard [16]. The analysis is performed using both linear and nonlinear wave theory. The utilization values of three most critical members in both the cases is shown in Table 4-11. The UC plots are shown in Figure 4-17 and Figure 4-18.

Table 4-11 Unity check values of critical members of Jacket

Member	UC _{linear wave}	UC _{nonlinear wave}	Difference (%)
Bracing	.824	0.837	1.57767
Bracing	.869	.872	0.34522
Bracing	.814	.833	2.33415
Leg A	.816	.817	0.1255



5. Case study – Part 2: Mass modelling approaches

The second and main objective of this thesis is to investigate various approaches of modelling Topside mass over the Jacket. This is generally required when the main focus of design is the Jacket structure with limited information and limited time is available for the Topside modelling. However not many guidelines are available on the approach to be used while modelling the Topside mass. Several approaches of modelling Topside mass are discussed in this section. The results for these approaches are compared and recommendations are made to the practicing engineers on the selection of best suited approach. All the approaches are first discussed and applied to a simple cantilever beam before applying to the complex Jacket structure.

5.1. Mass modelling approaches

This section presents the various approaches formulated to represent the mass of a structure. The structure can be as simple as a beam or can be complex as Topside. Three approaches are mainly formulated and discussed below.

Approach 1 – Density Approach

In this approach, the mass is modelled as structural elements with defined material density. The density can be increased for the material in order to achieve the targeted weight. The material density is converted to mass and assigned proportionally at the nearby nodes as masses in each of the three translational degrees of freedom.

Approach 2 – Point Loads as Mass Approach

The mass is modeled as point loads and these point loads are converted to masses in each of the three translational degrees of freedom. This means the point loads are contributing directly to the mass matrix of the considered system.

Approach 3 – Lumped Mass Approach

In this approach, the mass is modelled a lumped mass at the nodes. The lumped mass is assigned in all three translational degrees of freedom in order to capture the dynamic behavior more precisely. It is however worth mentioning here that the lumped mass approach is applicable only for the dynamic analysis and do not contribute to the static loading.

5.2. Mass modelling approaches demonstration on simple beam

The above mentioned approaches of modelling the mass are first applied to a simple beam before moving further to the complex Topside structure. The beam dimensions and material properties are shown below. These approaches of mass distribution are shown for 2 node, 4 node and 6 node beam. The beam is modelled in finite element software SAP2000 and natural frequencies of are obtained and compared for these approaches. Natural frequencies are also found out by doing manual calculations and also by using theoretical solutions for 6 node beam. Results are compared and conclusions are drawn in the end.

5.2.1. Section and material properties

The section chosen for this part of the case study is shown in **Error! Reference source not found.** and Figure 5-2. The section and material properties are shown in Table 5-1.

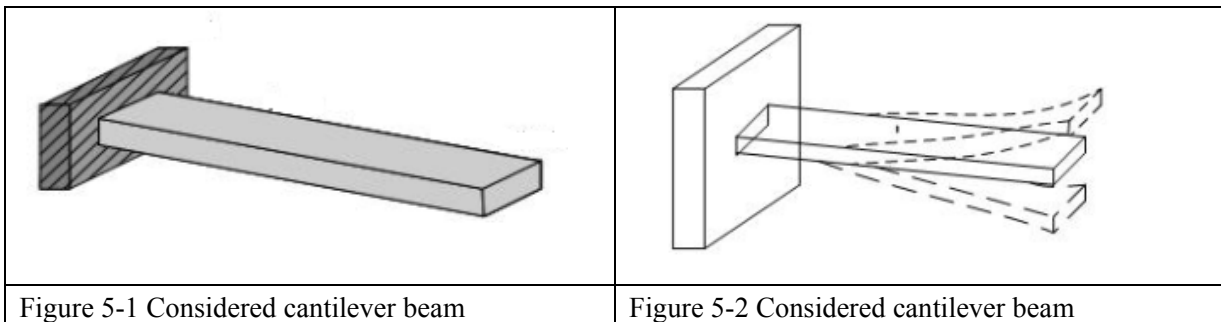


Table 5-1 Section and material properties of beam

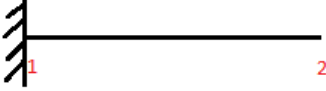
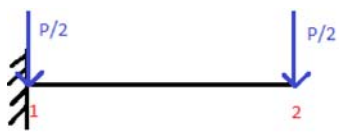
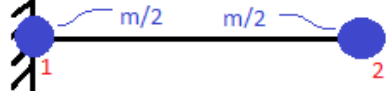
Section property	Value
Height , h	0.003 m
Width, b	0.02 m
Length , l	0.45 m
Material	S 355

5.2.2. Mass modelling approaches and analysis in SAP2000 - 2 nodes

The three approaches used for mass modelling is applied to the simple beam structure as shown in Table 5-2. It is to be noted that for approach 2 i.e. point loads, the point load at each node is converted to equivalent mass in all three translational degrees of freedom by the software. Also for

approach 3, lumped mass defined at each node is assigned in all three translational degrees of freedom.

Table 5-2 Mass modelling approaches demonstrated on a simple 2 node beam element

Approach 1	Approach 2	Approach 3
		
mass modelled as density density = 7850 kg/m ³ mass of beam, m = 0,212 kg	mass modelled as loads density = 0 P = m · g = 2,08N	Mass modelled as point masses density = 0 m = 0,212 kg

Results of static analysis in SAP2000-2 node case

Table 5-3 shows the static results for the three mass approaches on 2 node beam. The deflection at the tip of the cantilever is shown. The analytical solution for tip displacement is 2.50 mm and calculation is shown in Appendix A. It is seen that the analytical solution is matching with the approach 1. This is due to the fact that density is uniformly distributed throughout the length of the beam. However, displacement in approach 2 is on higher side since mass (converted from loads) is only acting at the end nodes. It is expected to get better results from approach 2 on discretizing the beam further into more number of finite elements as will be shown later.

It is also worth mentioning that the lumped mass approach doesn't yield any results for the static analysis results. This is possibly do due the fact that the lumped masses at the nodes are entering directly into the mass matrix and contribute only towards the dynamic behavior of the structure.

Table 5-3 Static displacement results for various approaches for 2 nodes case

Mass modelling approach	Tip displacement (SAP2000)	Analytical solution
Approach 1 (density as mass)	-2.50 mm	-2.50 mm
Approach 2 (point loads as mass)	-3.33 mm	
Approach 3 (lumped mass)	0 mm	

Results of Eigenvalue analysis in SAP2000- 2 node case

The results for Eigen value analysis from FE analysis is shown in Table 5-4. It is found that all the three approaches are giving same results. This is due to the fact that the mass distribution at the nodes in all degrees of freedom is similar in all the three approaches. However, the results are far away from the analytical solution due to less discretization of the beam section. It is expected to get better comparison of FE results with analytical solution on discretizing the section into more number of finite elements as is shown in later sections.

Table 5-4 Natural frequency comparison for 2 node element (vertical plane only)

2 node element	Mode shape	SAP2000 result	Analytical solution
Approach 1 (density as mass)	1	8.624	12.38
Approach 2 (point loads as mass)	1	8.624	12.38
Approach 3 (lumped mass)	1	8.624	12.38


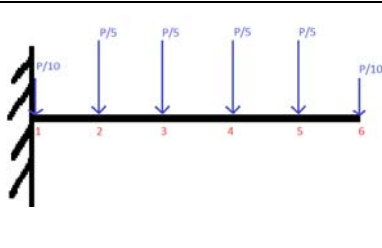
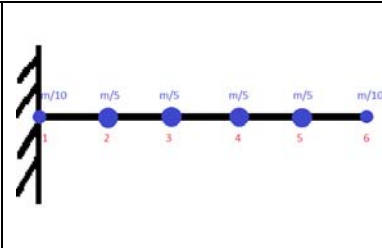
Note 1: Eigenvalue results from SAP2000 are found same for three mass modelling approaches

Note 2: SAP2000 results are deviating from analytical solution due to less discretization of section

5.2.3. Mass modelling approaches and analysis in SAP2000 - 6 nodes

The mass modelling approaches are now applied to 6 node beam as shown in Table 5-5.

Table 5-5 Mass modelling approaches demonstrated on a simple 6 node beam element

		
mass modelled as density density = 7850 kg/m ³ mass of beam, m = 0.212 kg	mass modelled as loads density = 0 $P = m \cdot g = 2.08\text{N}$	Mass modelled as point masses density = 0 m = 0.212 kg

Results of static analysis-6 node case

The results for static displacement is shown in Table 5-6. It is seen that the SAP2000 results matches more closely with the analytical solution due to better discretization in this case.

Table 5-6 Static displacement results for various approaches for 6 nodes case

Mass modelling approach	Tip displacement (SAP2000)	Analytical solution
Approach 1 (density as mass)	-2.50 mm	-2.50 mm
Approach 2 (point loads as mass)	-2.539 mm	
Approach 3 (lumped mass)	0 mm	

Results of Eigenvalue analysis from SAP2000- 6 node case

The results for Eigen value analysis from SAP analysis is shown in Table 5-7 for 6 node case. Similar to 2 node case, all three mass modelling approaches are giving same results.

Table 5-7 Natural frequency comparison for 6 node element (vertical plane only)

Mass modelling approach	Mode	SAP2000 result	Analytical solution
Approach 1 (density as mass)	1	12.155	12.38
	2	72.983	78.18
	3	196.902	217.16
Approach 2 (point loads as mass)	1	12.154	12.38
	2	72.975	78.18
	3	196.879	217.16
Approach 3 (lumped mass)	1	12.154	12.38
	2	72.975	78.18
	3	196.879	217.16

Note 1: Eigenvalue results from SAP2000 are found same for three mass modelling approaches

Note 2: Results are matching well (at-least for lower modes) from analytical solution due to more discretization

5.2.4. SAP2000 results comparison with numerical and analytical solution

The earlier sections (section 5.2.2 and 5.2.3) discussed the demonstration of mass modelling approaches on 2 node and 6 node beam section. It is concluded that the lumped mass approach (approach 3) does not contribute to static results and contributes directly to the mass matrix for the dynamic analysis. It is also concluded that the three approaches yields same results for Eigenvalue analysis. The results matches well with analytical solution at-least for the first few modes.

It is interesting to compare the SAP2000 results with numerical and analytical solutions. The SAP2000 results are found using the approach 1 (since all 3 approaches yields same results). The numerical calculation is based on FEM theory. The calculation is done in MATLAB software wherein the stiffness and mass matrices are formulated for each element and then assembled together to derive the global mass and the stiffness matrix. The natural frequencies of the beam section is then obtained using the Eigen value equation. The MATLAB code for 6 node beam can be found in Appendix B. The analytical solution is based on empirical relations and can be found in Appendix A. It is noted that only the vertical modes are compared in this study and comparison is made in Table 5-8 . It is seen that the values matches well for lower modes. The illustration of these modes is shown in Figure 5-3. The comparison of natural frequencies is shown in Figure 5-4 and Figure 5-5. The percentage error is shown in Figure 5-6.

Table 5-8 Frequency comparison of SAP2000 results with numerical and analytical solution

Mode	SAP 6 node	SAP 256 node	MATLAB 6 node	Analytical Solution
1 st	12.15	12.37	-	12.38
2 nd	72.98	77.56	78.80	78.18
3 rd	196.90	217.11	217.81	217.16
4 th	367.33	425.28	429.74	425.63
5 th	537.90	702.66	710.61	703.60
6 th	-	1049.0	1169.4	1051.1
7 th	-	1464.0	1683.5	1468.0
8 th	-	1947.5	2401.3	1954.4
9 th	-	2499.1	3395.5	2510.4
10 th	-	3118.4	5124.0	3135.8

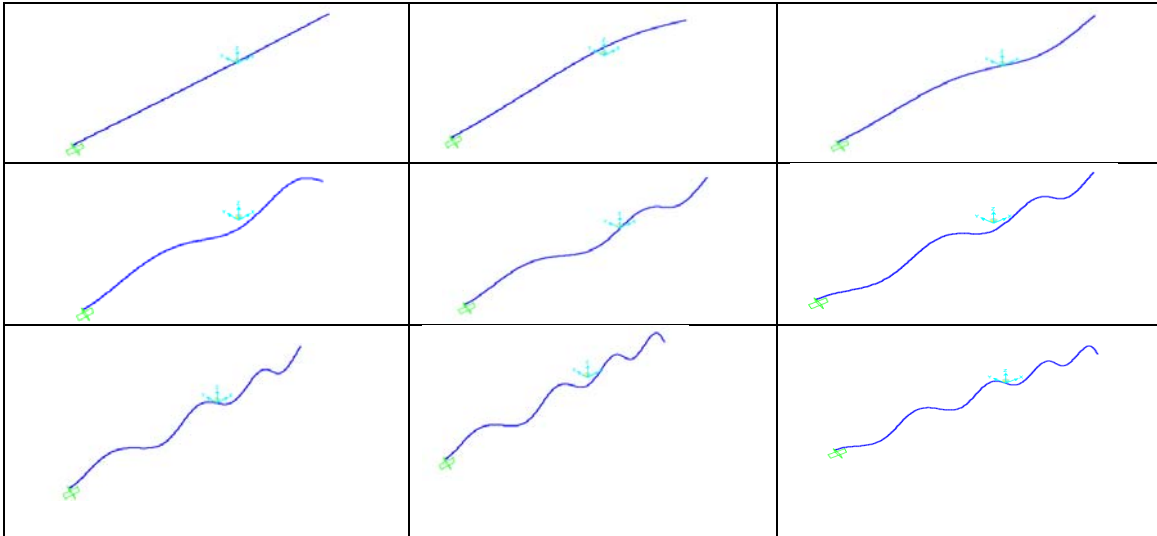


Figure 5-3 Mode shapes for the considered cantilever beam

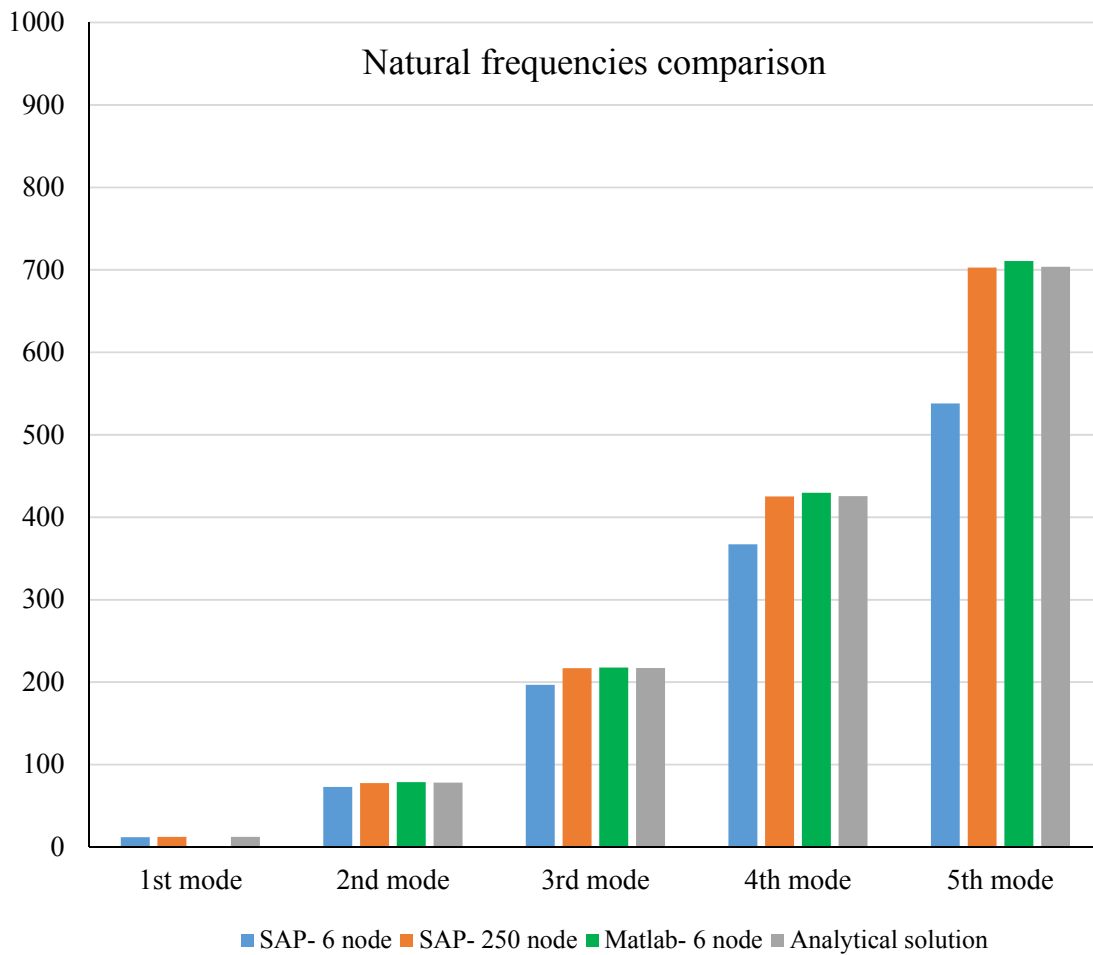


Figure 5-4 First 5 natural frequencies comparison

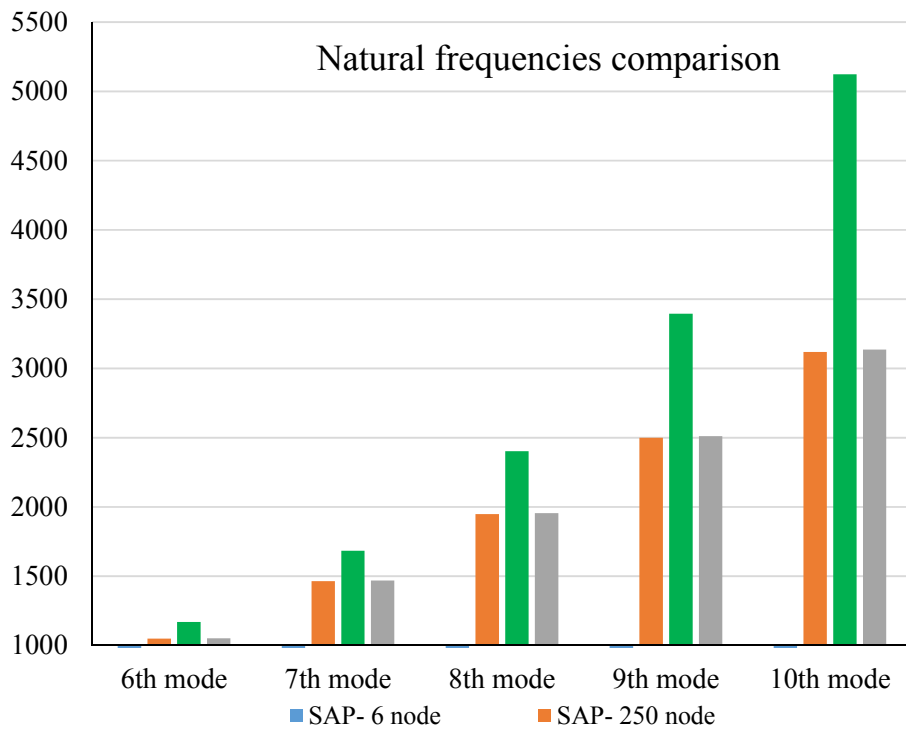


Figure 5-5 Mode 5 to mode 10 natural frequencies comparison

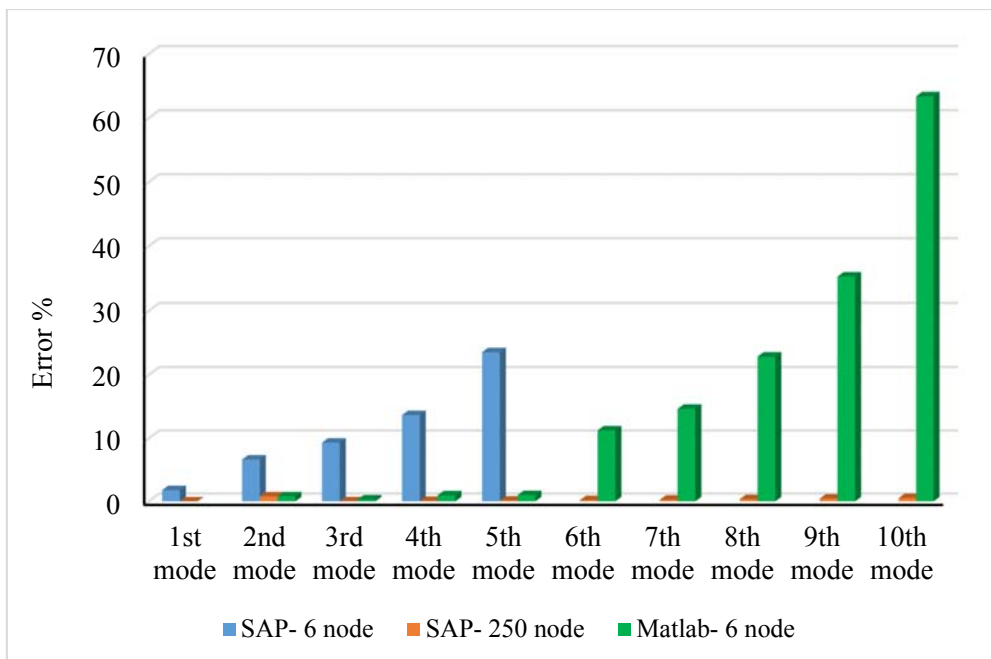


Figure 5-6 Error percentage in various approaches

5.3. Mass modelling approaches demonstration on Martin Linge Topside

The Topside for Martin Linge platform is one of the heaviest in the NCS region. For the Engineering contractor designing only the Jacket it becomes not only impractical but also uneconomical to spend many hours on modelling the Topside in detail. Also the currently available guidelines do not mention any procedures for modelling the Topside mass approximately without modelling each of its modules in detail. It is therefore intended to apply above discussed mass modelling approaches to the Martin Linge Topside and observe the structural response of the Jacket for various cases. In the end, results are discussed and recommendations are made to the practicing engineers on the selection of suitable mass modelling approach.

5.3.1. Topside models developed using mass modelling approaches

The three mass modelling approaches explained earlier on a simple beam is extended to the complex Martin Linge Topside structure. The main focus of this study is to investigate the effect of Topside modelling approach on the Jacket response. The Topside models are developed using the above discussed modelling approaches namely density increment, point loads as masses and lumped mass approach. For the lumped mass approach two cases are considered and is discussed later in detail. This section explains the Topside models developed using

Approach 1 – Density increment

The density increment mass modelling approach is applied to the Martin Linge Topside. This is the same model as explained earlier in Section 4.2.1. The complete model of the platform is shown in Figure 5-7.

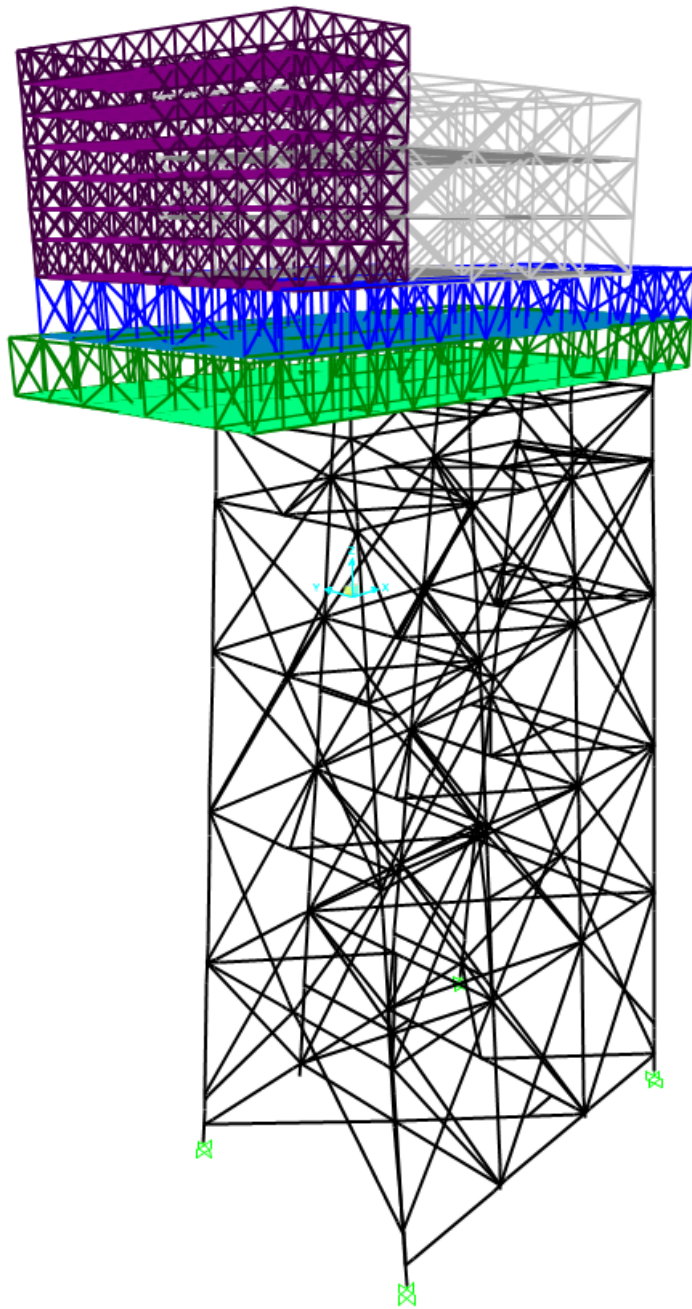
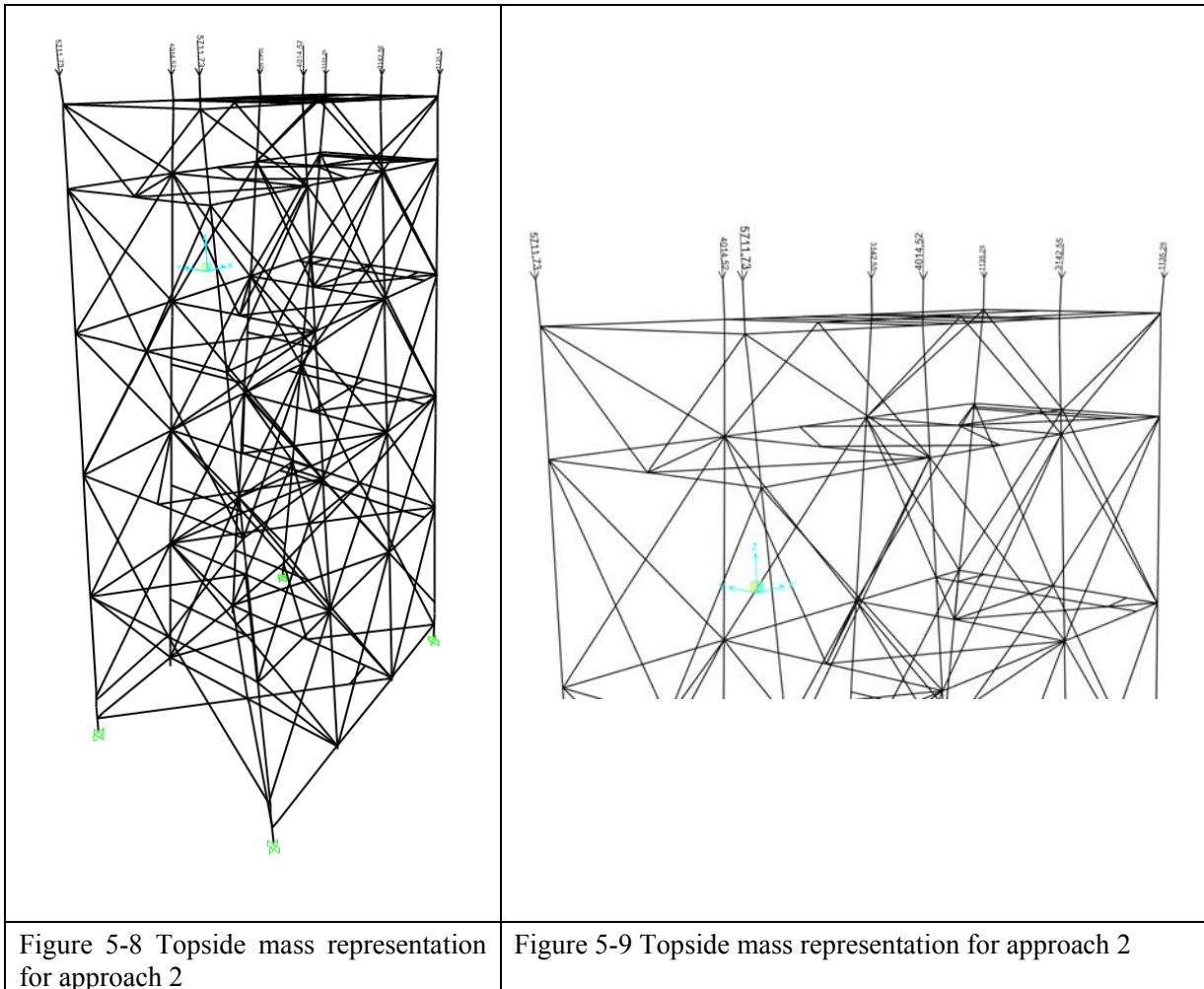


Figure 5-7 Topside model for density increment approach

Approach 2 – Point loads as masses

The Topside mass of 28000 tons is applied as point loads to the Jacket legs as shown in Figure 5-8 and Figure 5-9. The point loads are derived based on the module wise distribution of Topside mass and calculations are shown in Appendix C.



Approach 3 – Lumped masses

In this approach, the Topside mass is modelled as lumped masses at the CoG locations of each module. The lumped mass is then connected to the support points of the module using rigid beam sections so as to make a pyramid kind of structure with lumped mass at the top. Two cases are made for this lumped mass approach.

Case 1: In this case, the lumped masses are defined at the CoG location of each module. The mass assigned is equivalent to the module weight. The mass is supported on the pyramids connected to the supports of respective module. The detailed calculations of the masses and CoG locations is shown in Appendix C. The Topside model is shown in Figure 5-10. The complete model is shown in Figure 5-11 and Figure 5-12.

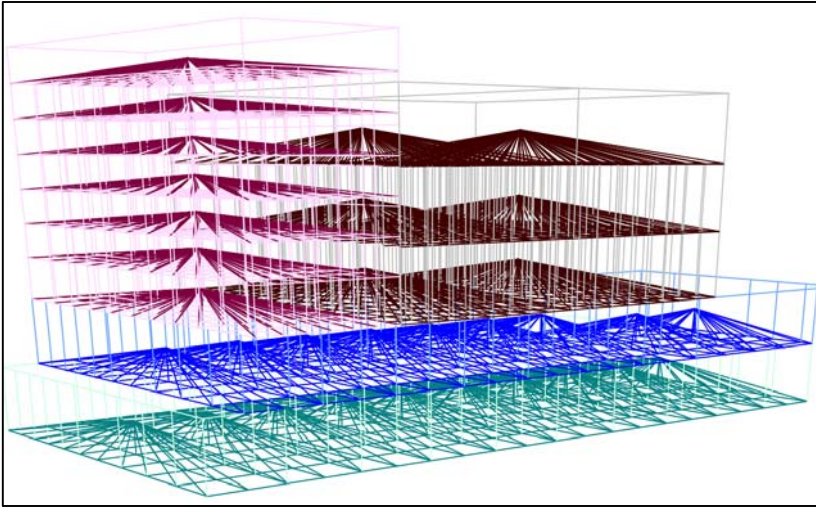
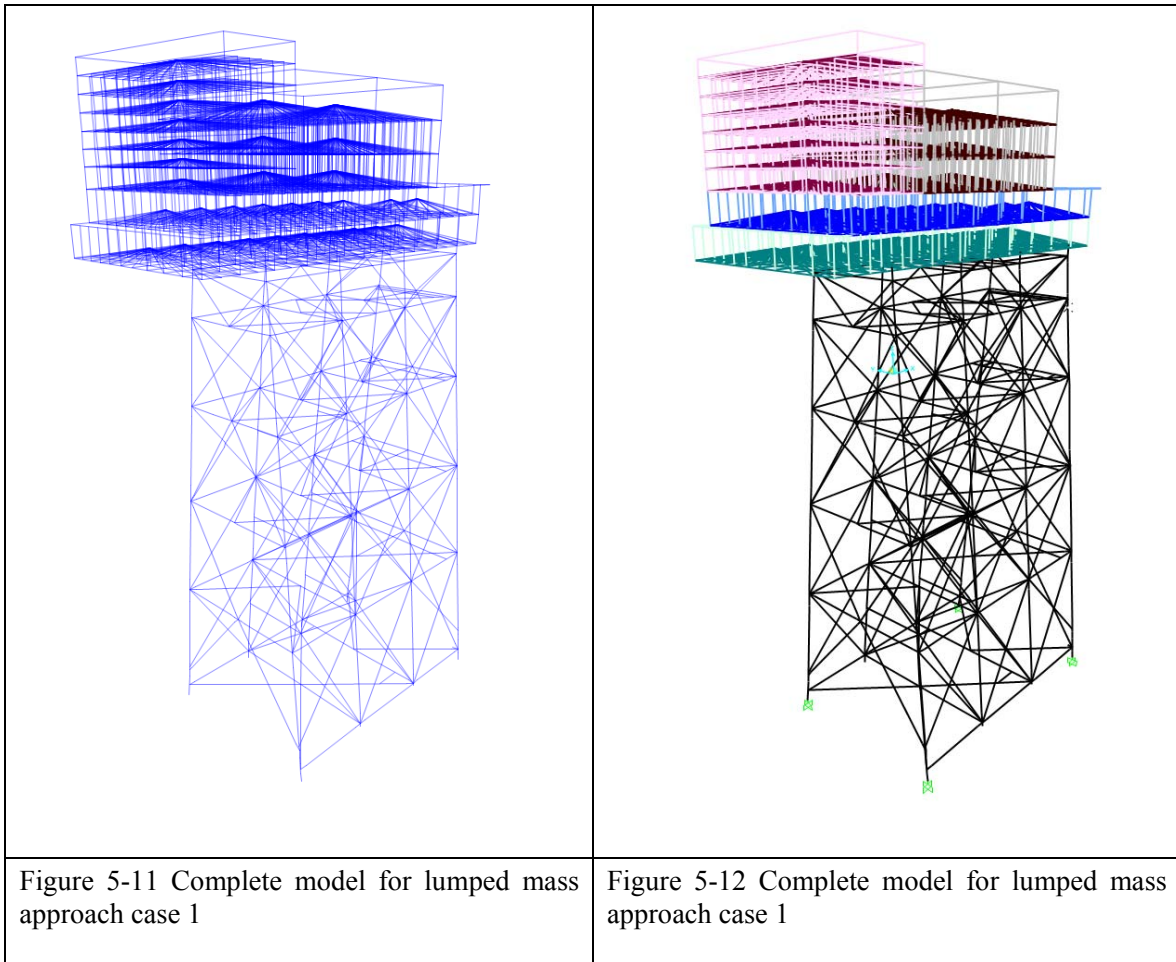


Figure 5-10 Topside model for lumped mass approach case 1



Case 2: In this case, the Topside mass is represented by just 3 big lumped masses. The motivation is to compare the results of this case as well as Topside modelling efforts are very less for this approach. The lumped mass and CoG calculations are shown in Appendix C. The Topside model is shown in Figure 5-13. The complete model is shown in Figure 5-14.

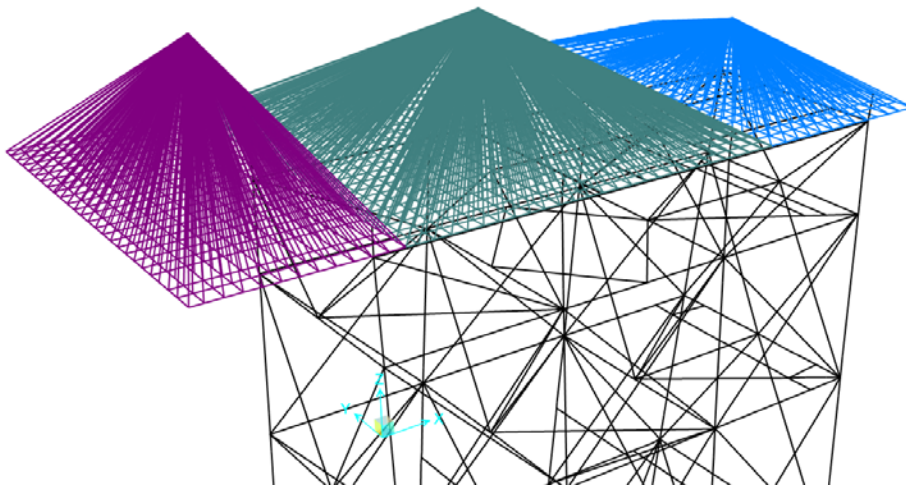


Figure 5-13 Topside model for lumped mass approach case 2

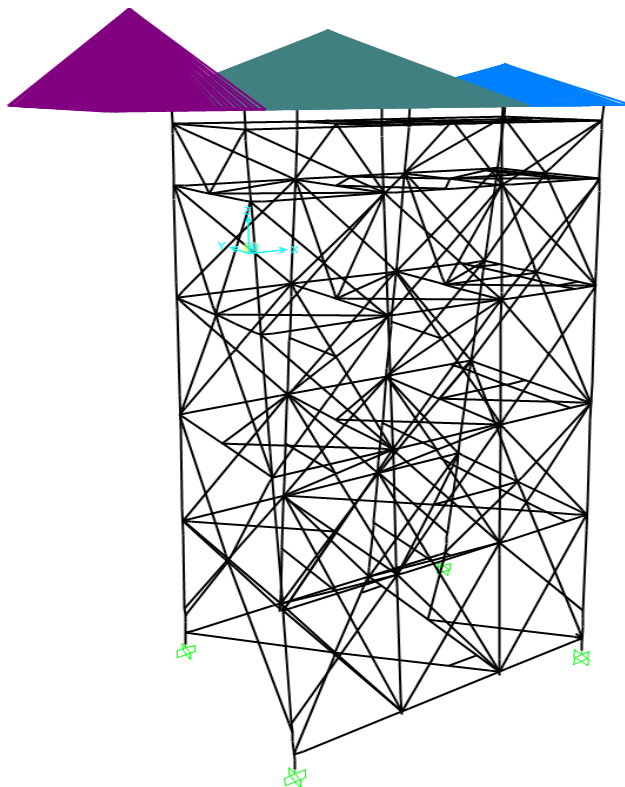


Figure 5-14 Complete model for lumped mass approach case 2

5.3.2. Results – Eigenvalue analysis

The eigenvalue analysis is performed on the 3 approaches and results for the time periods is shown in Table 5-9 and Figure 5-15.

Table 5-9 Natural time period of structure in various approaches

Mass modelling approach	Mode	SAP2000 result	Direction
Approach 1 – D I (density as mass)	1	3.00194	Sway - Y
	2	2.22642	Sway - X
	3	1.61245	Torsion
Approach 2 – P L (point loads as mass)	1	2.48813	Sway - Y
	2	2.14406	Sway - X
	3	1.57742	Torsion
Approach 3 – L M 1 (lumped mass – casa 1)	1	3.17588	Sway - Y
	2	2.97827	Sway - X
	3	1.45694	Torsion
Approach 3 – L M 2 (lumped mass – casa 2)	1	2.73803	Sway - Y
	2	1.94277	Sway - X
	3	1.23281	Torsion

Time periods Comparison for mass modellin approaches

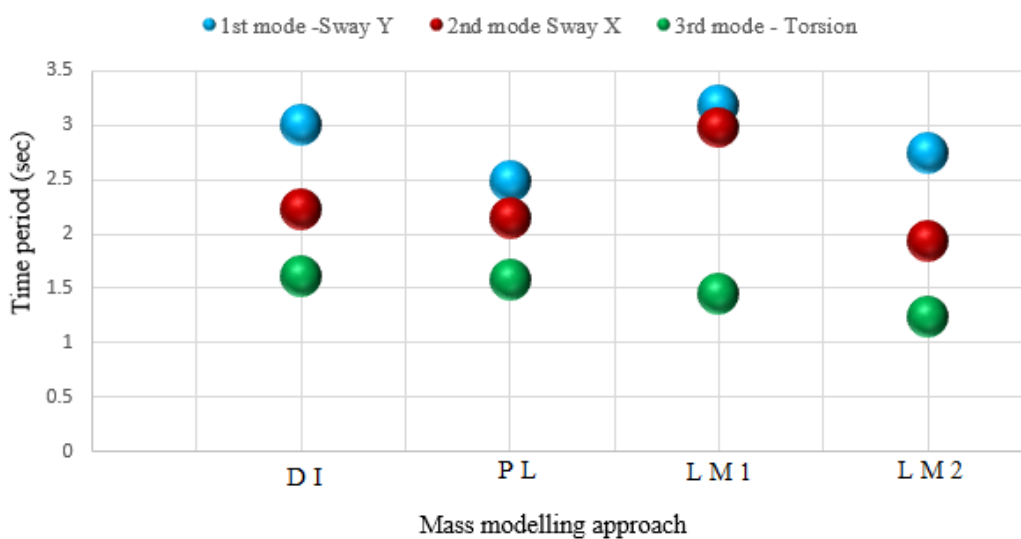


Figure 5-15 Natural time period for various mass modelling approaches – global modes

5.3.3. Results – Serviceability limit state (SLS)

The displacement for leg A of the Jacket is obtained for each of the mass modelling approaches and results are shown in Figure 5-16 and Figure 5-17

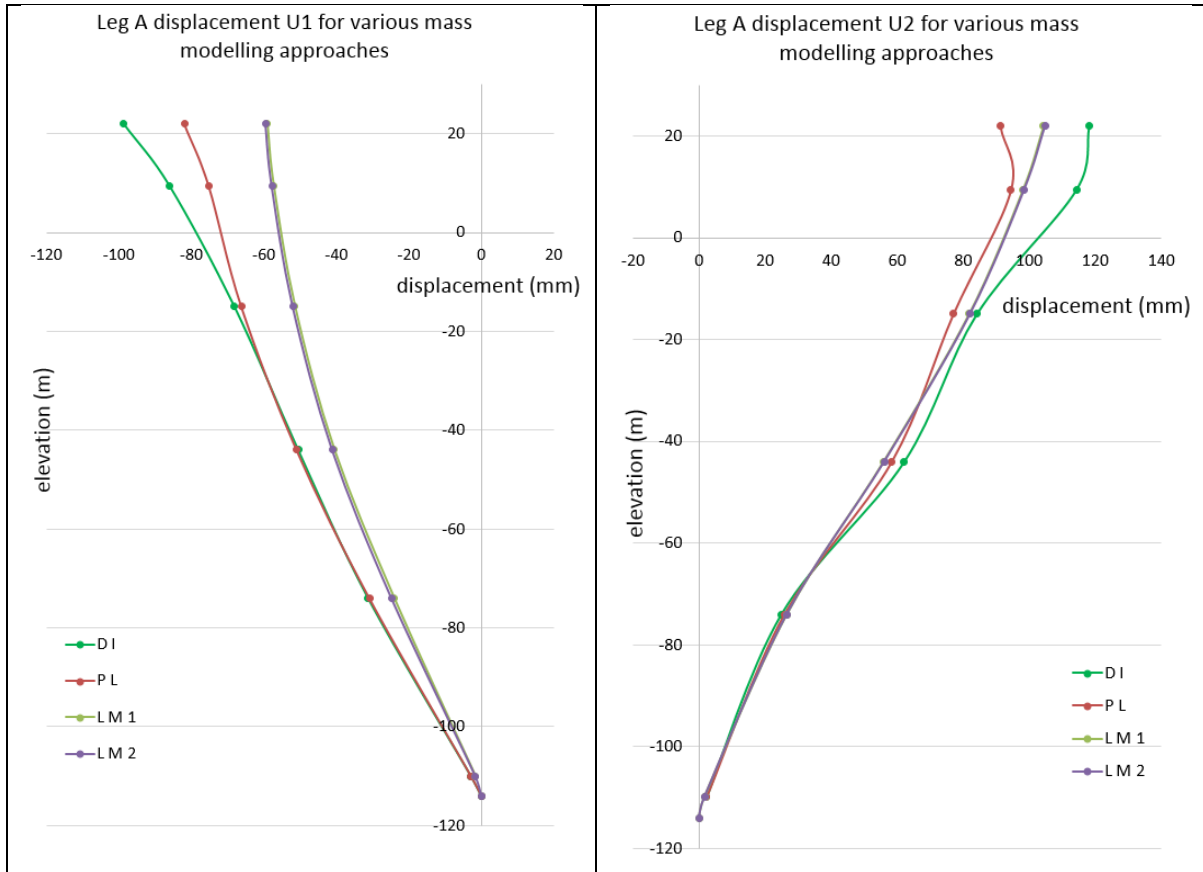


Figure 5-16 Leg A displacement U1 for various approaches – worst load combination

Figure 5-17 Leg A displacement U2 for various approaches – for worst load combination

5.3.4. Results – Ultimate limit state (ULS)

The utilization ratio in the leg A is found out for the various mass modelling approaches. The unity check values for each of the ULS load combination and mass modelling approach is shown in Table 5-10. The complete unity check plots for all members of the Jacket is shown in Figure 5-18 to Figure 5-21.

Table 5-10 UC values for leg A in various approaches

	ULS _A					ULS _B				
	1	2	3	4	5	1	2	3	4	5
DI	0.796	0.799	0.817	0.818	0.807	0.610	0.613	0.643	0.649	0.630
PL	0.600	0.601	0.618	0.627	0.611	0.459	0.462	0.594	0.608	0.541

Lump 1	0.153	0.135	0.227	0.231	0.200	0.269	0.216	0.321	0.310	0.247
Lump 2	0.157	0.138	0.227	0.233	0.205	0.279	0.223	0.320	0.312	0.253

Approach 1 - Density increment

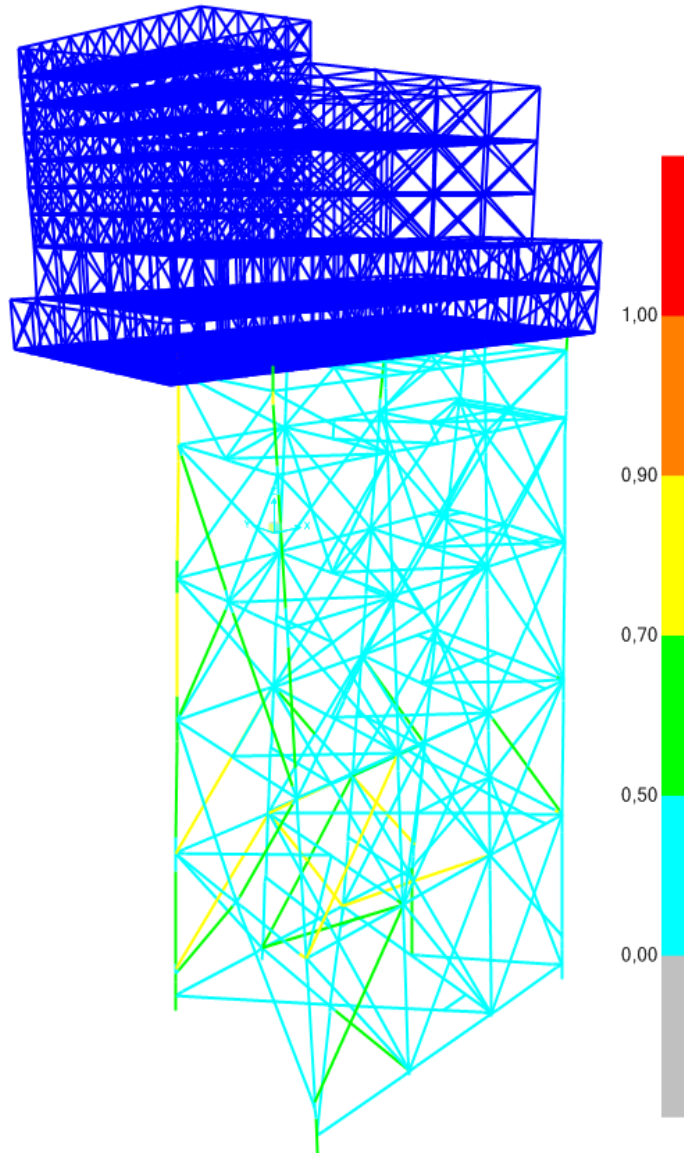


Figure 5-18 UC plot for Jacket – density increment approach

Approach 2 – Point loads as masses

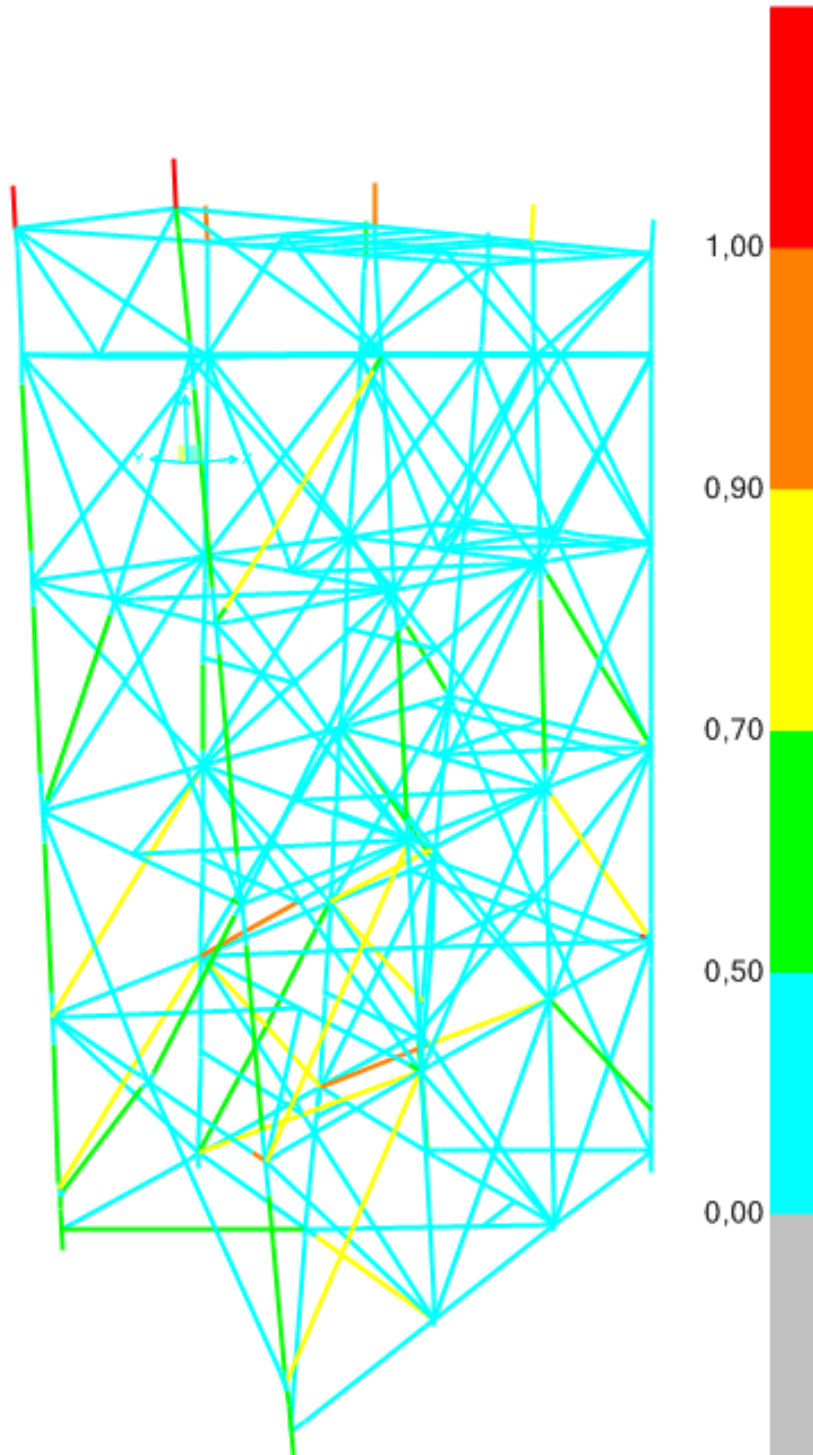


Figure 5-19 UC plot for Jacket – point loads approach

Approach 3 – Lumped mass case 1

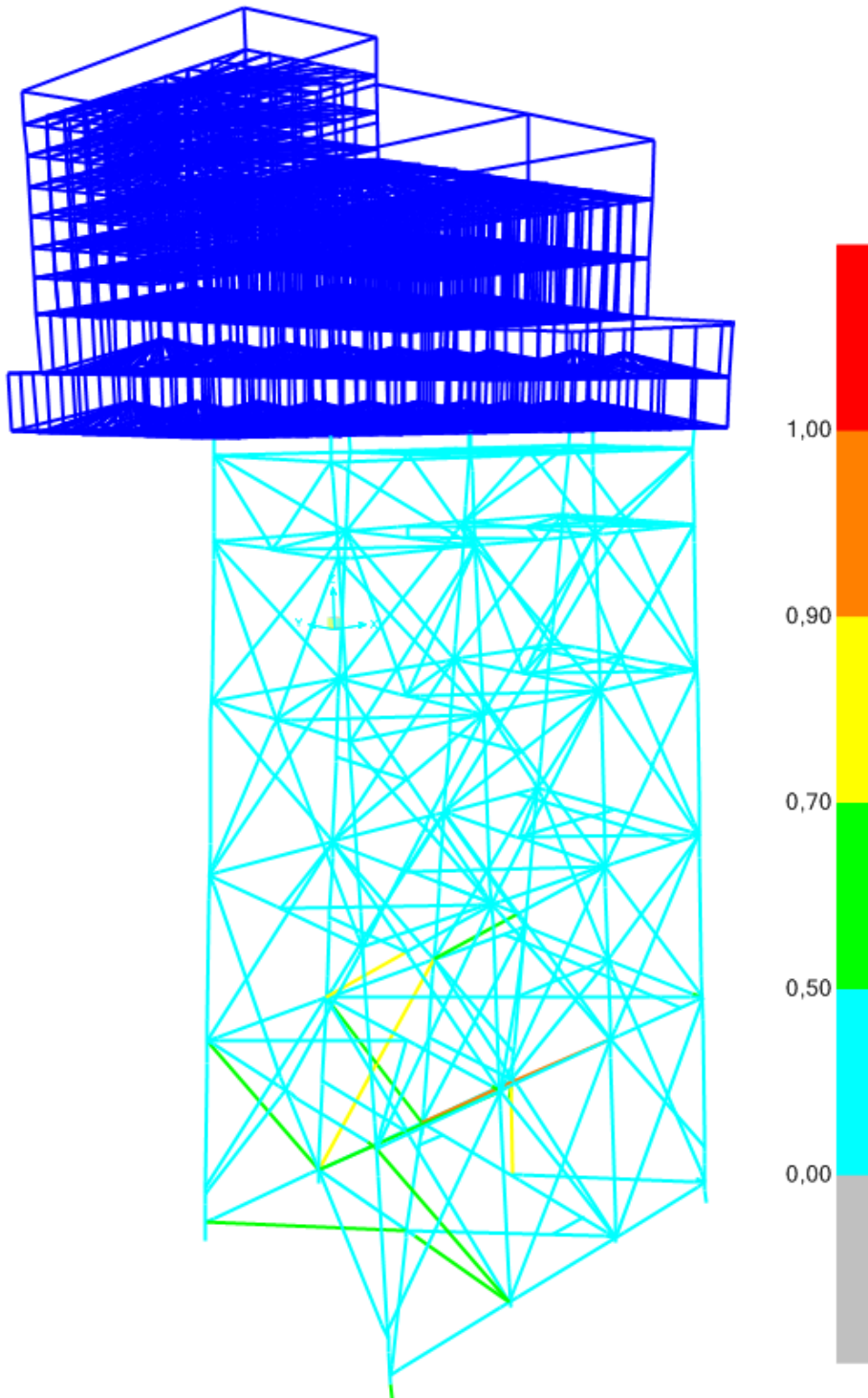


Figure 5-20 UC plot for Jacket – lumped mass approach case 1

Approach 3 – Lumped mass case 2

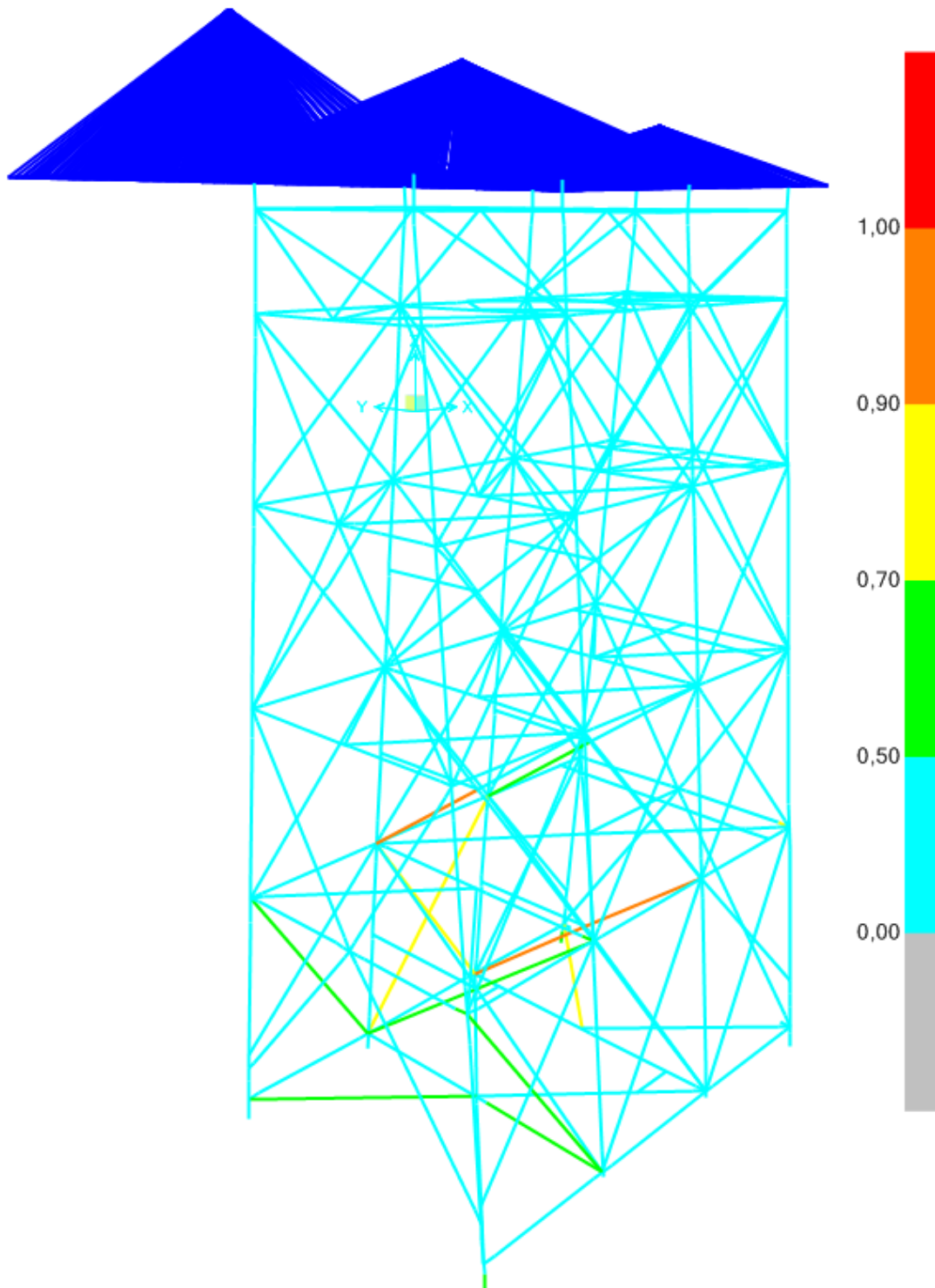


Figure 5-21 UC plot for Jacket – lumped mass approach case 2

6. Discussion and Conclusions

6.1. Discussion and Conclusions

In this thesis, the effect of the using linear and nonlinear wave theories on the structural response of an offshore structure is discussed. Also, the significance of modelling the Topside mass using various mass modelling approaches is highlighted.

The hydrodynamic loading is among the major loading when it comes to offshore structures. These loadings are derived from several available linear as well as nonlinear wave theories. All these wave theories have some underlying assumptions and it becomes very important for researchers and engineers to understand these assumptions carefully before applying any theory to a structure. Various assumptions behind the linear Airy's and nonlinear 5th order Stoke's theory are discussed in detail. The effect of these wave theories on the structural response of the structure is studied. The study is first done on a simple column structure and then extended to a big complex offshore platform. The platform chosen for the case study is Martin Linge platform and is one of the heaviest platforms in the Norwegian Continental Shelf. The platform weighs 38000 tons in total having a Topside of 28000 tons and a Jacket of 10000 tons. Both linear and nonlinear wave theory are used for the SLS and ULS analysis of the Jacket structure for a 100 year return period wave. The nonlinear Stoke's theory gives slightly higher values of the leg displacement for SLS analysis. Also, the unity check values in the members of the Jackets are higher when using the Stoke's theory for ULS analysis. This is probably because of the loading nonlinearities captured by the 5th order Stoke's theory. These nonlinearities are present due to the nonlinear drag force term and results in higher member forces, higher displacements and higher utilization values. The selection of a particular wave theory also depends on the water depth levels at the location of the structure as well as the wave parameters.

In case of heavy offshore structures like Martin Linge platform, the dead weight of the heavy Topside is also one of the governing factors for the Jacket design. It is seen in case of Martin Linge platform, that the Jacket design is completed even before the Topside design is finalized. In such cases it is very important to represent the Topside mass precisely for Jacket design even when the Topside weight details are not available in detail. Also often the Topside and Jacket are designed by separate design consultants. For the design consultant responsible for Jacket design, it becomes not only impractical but also uneconomical to spend hundreds of hours in modelling the Topsides

even when the details are available. The Topside mass in such cases is generally modelling in an approximate way. However, it is found that not many guidelines are available in the codes and standards on modelling the Topside mass approximately without compromising on the precision of the Jacket response. It is due to this fact that practicing engineers doing the Jacket design face problems while representing the Topside mass. This is identified as one of the major problems for this thesis work. To overcome this problem, an attempt is made to formulate various approaches and methodologies of modelling the Topside mass. These approaches are first demonstrated on a simple structure before extending the study to Martin Linge Topside.

Three mass modelling approaches are formulated and discussed in this thesis. The first approach is the density increment approach. In this approach, it is recommended to model only the primary and secondary members of modules without modelling any tertiary members. Also, the equipment and other weight on the module decks can be ignored. To account for the equipment and other dead weight loading on the module floor, it is recommended to increase the density of the primary and secondary members of the deck member in order to attain actual targeted mass.

The second mass modelling approach discussed is the point load approach wherein the point loads are applied as masses directly on the top of Jacket legs. This approach can be useful when very limited information is available for the Topside or very limited number of engineering hours is assigned to Topside mass modelling.

The third approach discussed is the lumped mass approach wherein the modules are represented by lumped masses at the CoG and are connected to the support points with rigid elements.

The three mass modelling approaches are applied on the heavy Martin Linge Topside. Eigenvalue and Static analysis is performed and Jacket response is observed. It is observed that the density increment approach gives fairly good results where the natural time periods are well separated for the first three global modes. This is probably because the mass representation is fairly accurate since the deck loading is represented by the increased density. Also, since primary and secondary members are modelled for the Topside, the stiffness is captured more precisely compared to all other approaches.

The point load approach is a very simplified approach. The natural periods for this approach are found to be lower especially for the first mode. This might be due to the Topside stiffness which is not represented correctly in this approach.

The lumped mass approach case one, wherein each module is represented overestimates the natural time periods by around 5% for mode 1 (sway Y) and 25% for mode 2 (sway Y). The overestimate is more for Y direction since the Jacket is slender in that direction. Also, since lumped mass is connected to the support points using pyramid rigid elements, the stiffness contribution is missing from the columns and deck elements. However, this approach can be useful to give an initial estimation of the structural response in event of lack of Topside data or number of engineering hours for modelling.

6.2. Scope of future work

The scope for future research is also identified. It is recommended to investigate the effect of other nonlinear linear wave theories on the structural response especially for Cnoidal and Stream function wave theory.

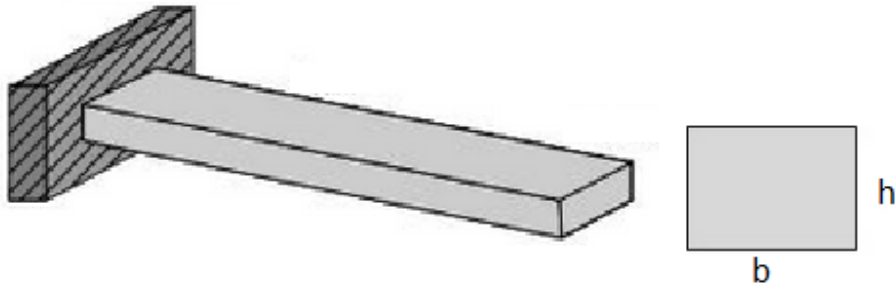
It is also recommended to verify the various proposed mass modelling approaches on couple of other case studies as well. This will not only reconfirm the conclusions but can also be very useful for upcoming standards and guidelines. The consideration of the Topside stiffness more precisely is also identified as future work. The point load case approach i.e. approach 2 can be tried by putting the point loads on the cellar deck support points rather than on the Jacket legs. This will take into account for Topside stiffness at-least to some extent if not completely.

7. References

- [1] Grosbard, A (2002). “Treadwell wharf in the summerland, California oil field: The first sea wells in petroleum exploration”, Oil-Industry History, Volume 3, Issue 1.
- [2] James, G (2015). “Offshore Platforms”, Subsea and Deepwater Oil and Gas Science and Technology, Gulf Professional Publishing, Boston.
- [3] Fenton, JD (1990). “Nonlinear wave theories”, In Eds. B. Le Mehaute and New York D.M. Hanes, Wiley, editors, The Sea, Vol.9: Ocean Engineering Science, 9-25
- [4] Gudmestad, O.T (2015). “Marine Technology and Operations: Theory and practice”, WIT press, Boston
- [5] Chakrabarti, SK (1987). “Hydrodynamics of offshore structures”, Computational Mechanics Publications, Boston.
- [6] Dean, RG and Dalrymple, RA (1991). “Water wave mechanics for engineers and scientists”, Advanced Series on Ocean Engineering, Volume 2, U.S.A.
- [7] Dean, RG (1974). “Evaluation and development of water wave theories for engineering application”, Vols 1 and 2, Spec. Rep. 1, U.S. Army, Coastal Engineering Research Center, Fort Belvoir, U.S.A.
- [8] Dean, RG (1970). “Relative validity of water wave theories”, Journal of Waterways Harbors, ASCE, 96, 105-119.
- [9] Computer & Structures, INC. (2016). *About SAP2000*, available online at: <https://www.csiamerica.com/products/sap2000> (accessed 14/06/2016).
- [10] Computer & Structures, INC. (2016). “SAP2000 analysis manual”
- [11] NORSOK (2007). “Actions and action effect”, N-003, September 2007.
- [12] Chopra, A (2007). “Dynamics of structures: Theory and applications to earthquake engineering”, 3rd edition, Prentice-Hall, New Jersey.
- [13] Rao, S (2011). “Mechanical Vibrations”, 5th edition, Prentice-Hall, Singapore.
- [14] R. Clough and J. Penzien (1975), “Dynamics of structures”, 2nd edition, McGraw-Hill, Inc. ISBN 0-07-011394-7.
- [15] NORSOK (2010). “Integrity of offshore structures”, N-001, June 2010.
- [16] NORSOK (2004). “Design of steel structures”, N-004, October 2004.

Appendix A – Analytical calculations for simple beam

Illustration of cantilever rectangular beam



Dimensions	Lengths
L	0.45m
b	0.02m
h	0.003m

Material properties	Density [kg/m ³]	Young's Modulus [N/m ²]
Steel	7850	2.1*10 ¹¹

Calculation of tip displacement for a simple cantilever beam

Mass per meter

$$m_x = \rho_{steel} \cdot b \cdot h \quad m = 7850 \frac{kg}{m^3} \cdot 0.02m \cdot 0.003m \quad m = 0.471 \frac{kg}{m}$$

Mass converted to newton

$$q = m \cdot g \quad q = 0.471 \frac{kg}{m} \cdot 9.81 \frac{m}{s^2} \quad q = 4.62051 \frac{N}{m}$$

Moment of inertia for a rectangular element

$$I = \frac{b \cdot h^3}{12} \quad I = \frac{0.02m \cdot (0.003m)^3}{12} \quad I = 4.5 \cdot 10^{-11} m^4$$

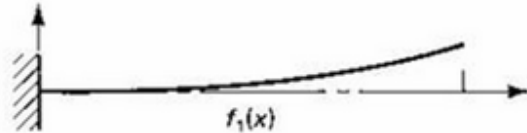
Tip displacement

$$\delta_{max} = \frac{q \cdot L^4}{8 \cdot EI} \quad \delta_{max} = \frac{4.62051 \frac{N}{m} \cdot (0.45m)^4}{8 \cdot 2.1 \cdot 10^{11} \frac{N}{m^2} \cdot 4.5 \cdot 10^{-11} m^4} \quad \delta_{max} = 0.0025m$$

$$\delta_{max} = 2.506mm$$

Analytical frequency solutions for a undamped 2D cantilever beam

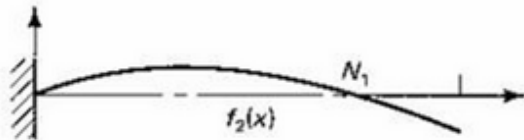
Mode shape 1 - Global mode



Analytical natural frequency, ω

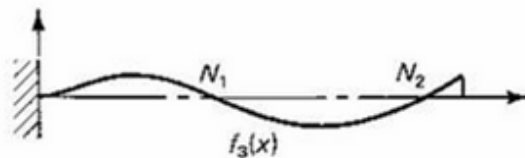
$$\omega_1 = (1.875)^2 \cdot \sqrt{\frac{E \cdot I}{m \cdot L^4}}$$

Mode shape 2 - Local mode



$$\omega_2 = (4.694)^2 \cdot \sqrt{\frac{E \cdot I}{m \cdot L^4}}$$

Mode shape 3 - Local mode



$$\omega_3 = (7.855)^2 \cdot \sqrt{\frac{E \cdot I}{m \cdot L^4}}$$

Analytical frequency solution for first three modes

Natural frequency

$$\omega_1 = (1.875)^2 \cdot \sqrt{\frac{2.1 \cdot 10^{11} \frac{N}{m^2} \cdot 4.5 \cdot 10^{-11} m^4}{0.471 \frac{kg}{m} \cdot (0.45m)^4}} = 77,77 \frac{rad}{s}$$

Frequency

$$f_1 = 12.37Hz$$

$$\omega_2 = (4.694)^2 \cdot \sqrt{\frac{2.1 \cdot 10^{11} \frac{N}{m^2} \cdot 4.5 \cdot 10^{-11} m^4}{0.471 \frac{kg}{m} \cdot (0.45m)^4}} = 489.28 \frac{rad}{s}$$

$$f_2 = 77.53Hz$$

$$\omega_3 = (7.855)^2 \cdot \sqrt{\frac{2.1 \cdot 10^{11} \frac{N}{m^2} \cdot 4.5 \cdot 10^{-11} m^4}{0.471 \frac{kg}{m} \cdot (0.45m)^4}} = 1364.81 \frac{rad}{s}$$

$$f_3 = 217.20Hz$$

Appendix B -MATLAB code for 6 node beam (2D element)

nodal beam element

%The frequencies are only developed for the x-z-plane as there are only 2 nodes acting in each node (translational and z direction).

```
E=2.1e11      %Youngs modulus in N/m^2
b=0.02        %Width of c/s in m
h=0.003       %Height of c/s in m
I=(b*h^3)/12  %Moment of inertia in m^4
L=0.45        %Total length of the beam in m
L1=L/5        %Length of beam element 1,2,3,4,5
rho=7850      %density of the beam in kg/m^3
m=rho*b*h*L   %Total mass of the beam in kg
```

%MASS MATRICES

%Here the constant in front of the mass matrix is calculated which is constant %for all the local beams

```
mConst=(rho*b*h*L1)/420
```

%Local mass matrix of element 1

```
m1=mConst*[156    22*L1    54    -13*L1    0 0 0 0 0 0 0 0 0 0;
            22*L1    4*L1^2    13*L1    -3*L1^2    0 0 0 0 0 0 0 0 0 0;
            54     13*L1    156    -22*L1    0 0 0 0 0 0 0 0 0 0;
            -13*L1  -3*L1^2  -22*L1    4*L1^2    0 0 0 0 0 0 0 0 0 0;
            0      0      0      0      0 0 0 0 0 0 0 0 0 0;
            0      0      0      0      0 0 0 0 0 0 0 0 0 0;
            0      0      0      0      0 0 0 0 0 0 0 0 0 0;
            0      0      0      0      0 0 0 0 0 0 0 0 0 0;
            0      0      0      0      0 0 0 0 0 0 0 0 0 0;
            0      0      0      0      0 0 0 0 0 0 0 0 0 0;
            0      0      0      0      0 0 0 0 0 0 0 0 0 0;
            0      0      0      0      0 0 0 0 0 0 0 0 0 0;
            0      0      0      0      0 0 0 0 0 0 0 0 0 0;
            0      0      0      0      0 0 0 0 0 0 0 0 0 0;
            0      0      0      0      0 0 0 0 0 0 0 0 0 0;]
```

%Local mass matrix of element 2

```
m2=mConst*[0 0 0    0    0    0    0 0 0 0 0 0 0 0;
            0 0 0    0    0    0    0 0 0 0 0 0 0 0;
            0 0 156    22*L1    54    -13*L1    0 0 0 0 0 0 0 0;
            0 0 22*L1    4*L1^2    13*L1    -3*L1^2    0 0 0 0 0 0 0 0;
            0 0 54     13*L1    156    -22*L1    0 0 0 0 0 0 0 0;
            0 0 -13*L1  -3*L1^2  -22*L1    4*L1^2    0 0 0 0 0 0 0 0;
            0 0 0      0      0      0      0 0 0 0 0 0 0 0;
            0 0 0      0      0      0      0 0 0 0 0 0 0 0;
            0 0 0      0      0      0      0 0 0 0 0 0 0 0;
            0 0 0      0      0      0      0 0 0 0 0 0 0 0;
            0 0 0      0      0      0      0 0 0 0 0 0 0 0;
            0 0 0      0      0      0      0 0 0 0 0 0 0 0;
            0 0 0      0      0      0      0 0 0 0 0 0 0 0;
            0 0 0      0      0      0      0 0 0 0 0 0 0 0;
            0 0 0      0      0      0      0 0 0 0 0 0 0 0;]
```

```

%Local mass matrix of element 3
m3=mConst*[0 0 0 0 0      0      0      0      0 0 0 0;
            0 0 0 0 0      0      0      0      0 0 0 0;
            0 0 0 0 0      0      0      0      0 0 0 0;
            0 0 0 0 0      0      0      0      0 0 0 0;
            0 0 0 0 156    22*L1    54    -13*L1  0 0 0 0;
            0 0 0 0 22*L1  4*L1^2   13*L1  -3*L1^2  0 0 0 0;
            0 0 0 0 54     13*L1    156    -22*L1  0 0 0 0;
            0 0 0 0 -13*L1 -3*L1^2 -22*L1  4*L1^2  0 0 0 0;
            0 0 0 0 0      0      0      0      0 0 0 0;
            0 0 0 0 0      0      0      0      0 0 0 0;
            0 0 0 0 0      0      0      0      0 0 0 0;
            0 0 0 0 0      0      0      0      0 0 0 0;]

```

```

%Local mass matrix of element 4
m4=mConst*[0 0 0 0 0 0 0      0      0      0 0;
            0 0 0 0 0 0 0      0      0      0 0;
            0 0 0 0 0 0 0      0      0      0 0;
            0 0 0 0 0 0 0      0      0      0 0;
            0 0 0 0 0 0 0      0      0      0 0;
            0 0 0 0 0 0 0      0      0      0 0;
            0 0 0 0 0 0 156    22*L1    54    -13*L1  0 0;
            0 0 0 0 0 0 22*L1  4*L1^2   13*L1  -3*L1^2  0 0;
            0 0 0 0 0 0 54     13*L1    156    -22*L1  0 0;
            0 0 0 0 0 0 -13*L1 -3*L1^2 -22*L1  4*L1^2  0 0;
            0 0 0 0 0 0 0      0      0      0      0 0;
            0 0 0 0 0 0 0      0      0      0      0 0;]

```

```

%Local mass matrix of element 5
m5=mConst*[0 0 0 0 0 0 0 0 0      0      0      0;
            0 0 0 0 0 0 0 0 0      0      0      0;
            0 0 0 0 0 0 0 0 0      0      0      0;
            0 0 0 0 0 0 0 0 0      0      0      0;
            0 0 0 0 0 0 0 0 0      0      0      0;
            0 0 0 0 0 0 0 0 0      0      0      0;
            0 0 0 0 0 0 0 0 0      0      0      0;
            0 0 0 0 0 0 0 0 0      0      0      0;
            0 0 0 0 0 0 0 0 0      0      0      0;
            0 0 0 0 0 0 0 0 156    22*L1    54    -13*L1;
            0 0 0 0 0 0 0 0 22*L1  4*L1^2   13*L1  -3*L1^2;
            0 0 0 0 0 0 0 0 54     13*L1    156    -22*L1;
            0 0 0 0 0 0 0 0 -13*L1 -3*L1^2 -22*L1  4*L1^2;]

```

```

%Global mass matrix
%Combining the local stiffnesses into a global mass matrix
M=m1+m2+m3+m4+m5

```

```

%STIFFNESS MATRICES
%Here the constant in front of the stiffness matrix is calculated which is
%constant %for all the local beams
kConst=(E*I)/(L1^3);

```

```

%Local stiffnes matrix of element 1
k1=kConst*[12    6*L1   -12    6*L1    0 0 0 0 0 0 0 0;
           6*L1   4*L1^2 -6*L1  2*L1^2  0 0 0 0 0 0 0 0;
           -12   -6*L1   12    -6*L1   0 0 0 0 0 0 0 0;
           6*L1  2*L1^2 -6*L1  4*L1^2  0 0 0 0 0 0 0 0;
           0     0     0     0     0 0 0 0 0 0 0 0;
           0     0     0     0     0 0 0 0 0 0 0 0;
           0     0     0     0     0 0 0 0 0 0 0 0;
           0     0     0     0     0 0 0 0 0 0 0 0;
           0     0     0     0     0 0 0 0 0 0 0 0;
           0     0     0     0     0 0 0 0 0 0 0 0;
           0     0     0     0     0 0 0 0 0 0 0 0;
           0     0     0     0     0 0 0 0 0 0 0 0;]

```

```

%Local stiffnes matrix of element 2
k2=kConst*[0 0 0    0    0    0    0 0 0 0 0 0;
           0 0 0    0    0    0    0 0 0 0 0 0;
           0 0 12   6*L1   -12   6*L1   0 0 0 0 0 0;
           0 0 6*L1  4*L1^2 -6*L1  2*L1^2  0 0 0 0 0 0;
           0 0 -12   -6*L1   12   -6*L1   0 0 0 0 0 0;
           0 0 6*L1  2*L1^2 -6*L1  4*L1^2  0 0 0 0 0 0;
           0 0 0    0    0    0    0 0 0 0 0 0;
           0 0 0    0    0    0    0 0 0 0 0 0;
           0 0 0    0    0    0    0 0 0 0 0 0;
           0 0 0    0    0    0    0 0 0 0 0 0;
           0 0 0    0    0    0    0 0 0 0 0 0;
           0 0 0    0    0    0    0 0 0 0 0 0;]

```

```

%Local stiffnes matrix of element 3
k3=kConst*[0 0 0 0 0    0    0    0    0 0 0 0;
           0 0 0 0 0    0    0    0    0 0 0 0;
           0 0 0 0 0    0    0    0    0 0 0 0;
           0 0 0 0 0    0    0    0    0 0 0 0;
           0 0 0 0 12   6*L1   -12   6*L1   0 0 0 0;
           0 0 0 0 6*L1  4*L1^2 -6*L1  2*L1^2  0 0 0 0;
           0 0 0 0 -12   -6*L1   12   -6*L1   0 0 0 0;
           0 0 0 0 6*L1  2*L1^2 -6*L1  4*L1^2  0 0 0 0;
           0 0 0 0 0    0    0    0    0 0 0 0;
           0 0 0 0 0    0    0    0    0 0 0 0;
           0 0 0 0 0    0    0    0    0 0 0 0;
           0 0 0 0 0    0    0    0    0 0 0 0;]

```

```

%Local Stiffness matrix of element 4
k4=kConst*[0 0 0 0 0 0 0 0 0 0 0 0;
            0 0 0 0 0 0 0 0 0 0 0 0;
            0 0 0 0 0 0 0 0 0 0 0 0;
            0 0 0 0 0 0 0 0 0 0 0 0;
            0 0 0 0 0 0 0 0 0 0 0 0;
            0 0 0 0 0 0 12 6*L1 -12 6*L1 0 0;
            0 0 0 0 0 0 6*L1 4*L1^2 -6*L1 2*L1^2 0 0;
            0 0 0 0 0 0 -12 -6*L1 12 -6*L1 0 0;
            0 0 0 0 0 0 6*L1 2*L1^2 -6*L1 4*L1^2 0 0;
            0 0 0 0 0 0 0 0 0 0 0 0;
            0 0 0 0 0 0 0 0 0 0 0 0;]

%Local stiffness matrix element 5
k5=kConst*[0 0 0 0 0 0 0 0 0 0 0 0;
            0 0 0 0 0 0 0 0 0 0 0 0;
            0 0 0 0 0 0 0 0 0 0 0 0;
            0 0 0 0 0 0 0 0 0 0 0 0;
            0 0 0 0 0 0 0 0 0 0 0 0;
            0 0 0 0 0 0 0 0 0 0 0 0;
            0 0 0 0 0 0 0 0 0 0 0 0;
            0 0 0 0 0 0 0 0 0 0 0 0;
            0 0 0 0 0 0 0 0 12 6*L1 -12 6*L1;
            0 0 0 0 0 0 0 0 6*L1 4*L1^2 -6*L1 2*L1^2;
            0 0 0 0 0 0 0 0 -12 -6*L1 12 -6*L1;
            0 0 0 0 0 0 0 0 6*L1 2*L1^2 -6*L1 4*L1^2;]

%Combining the local stiffnesses into a global stiffness matrix

K=k1+k2+k3+k4+k5

%Solving the eigen values for the beam for  $[M'+K]*x=0$  where
% $\{x\}'=-\omega^2\{x\}$ . This gives  $-[M]*\{x\}*\omega^2=-K*\{x\} \Rightarrow \omega^2=[M^{-1}]*[K]$ ,
%where  $\omega^2=\lambda$ 

M_inv=inv(M)
lambda=K*M_inv
[D]=eig(lambda)

%f= $\omega/(2*PI)$ , only the first 10 values are giving good estimations. The
%global frequency in z-direction is not coming out as a result.
for i=1:1:10
    omega(i,1)=sqrt(D(i,1))
    frequency(i,1)=(1/(2*pi))*omega(i,1)
end

```

Appendix C - CoG calculations for the Toppide modules

Approach 3 Lumped mass case

The lump masses is divided into three different masses. The masses are assumed to be uniformly distributed as it is in approach – 1 resulting in CoG's for each section module to be in the center. Local coordinates are defined at the left bottom corner of each lump mass. The figures display all platform modules considered and how its divided into different lump masses.

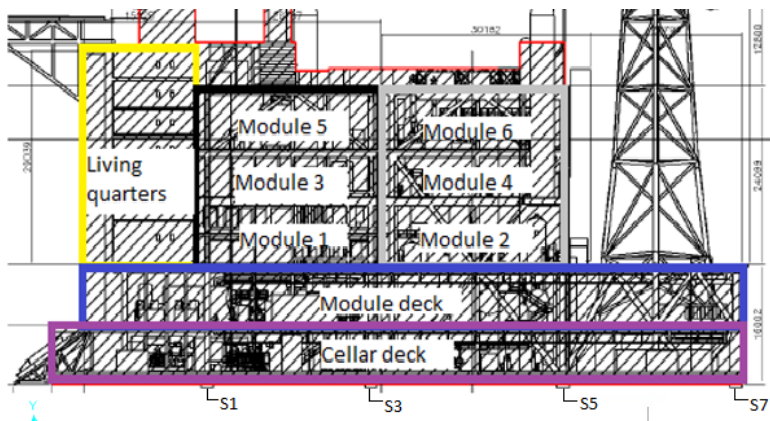


Figure 1 Toppide modules

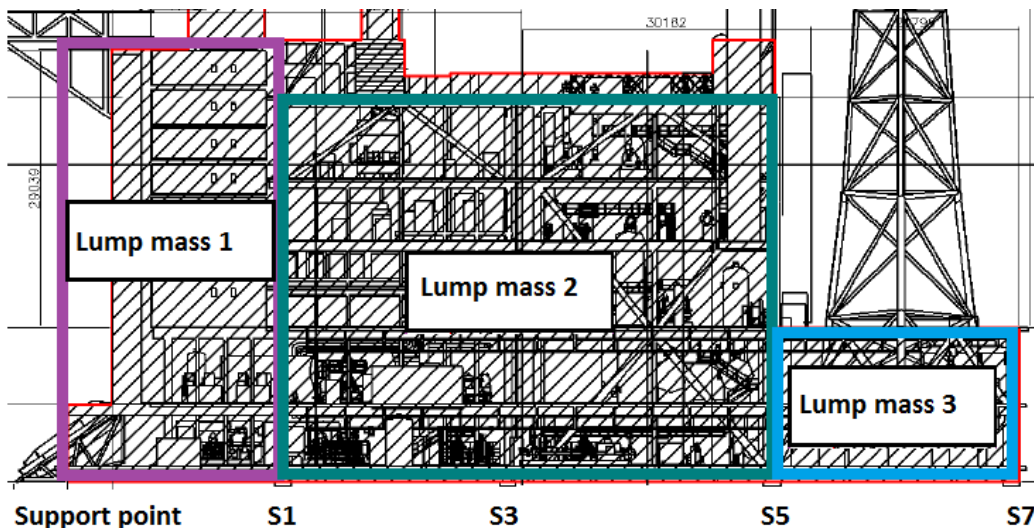


Figure 2 Toppide modules

CoG formulas:

$$\text{x-direction: } x = \frac{\sum m_i \cdot x_i}{m_{tot}}$$

$$\text{y-direction: } y = \frac{\sum m_i \cdot y_i}{m_{tot}}$$

$$\text{z-direction: } z = \frac{\sum m_i \cdot z_i}{m_{tot}}$$

A few abbreviations:

m_c - lump mass contribution of cellar deck

m_{mod} - lump mass contribution of module deck

m_{LQ} - lump mass contribution of living quarters

m_{1-6} - Total lump mass contribution of module 1-6

Lump mass 1 calculations

Local coordinate defined at the far tip of the platform (Living quarters side).

Lump Mass 1	Cellar deck	Module deck	Living Quarters
Lump mass area [m ²]	1175	925	980,5
Total area [m ²]	4975	4325	980,5
Ratio $\left[\frac{\text{m}^2}{\text{m}^2} \right]$	0,23618	0,21387	1,00
Total mass [ton]	8364,4	12409,1	2776,9
Lump mass weight [ton]	1975, 5	2654, 0	2776, 9

$$x = \frac{(m_c \cdot x_c + m_{mod} \cdot x_{mod} + m_{LQ} \cdot x_{LQ})}{m_c + m_{mod} + m_{LQ}}$$

$$\mathbf{x = 13,583m}$$

$$y = \frac{(m_c \cdot y_c + m_{\text{mod}} \cdot y_{\text{mod}} + m_{\text{LQ}} \cdot y_{\text{LQ}})}{m_c + m_{\text{mod}} + m_{\text{LQ}}}$$

$$y = \underline{24,438\text{m}}$$

$$z = \frac{(m_c \cdot z_c + m_{\text{mod}} \cdot z_{\text{mod}} + m_{\text{LQ}} \cdot z_{\text{LQ}})}{m_c + m_{\text{mod}} + m_{\text{LQ}}}$$

$$z = \underline{16,802\text{m}}$$

Lump mass 2 calculations

Local coordinate at support point S1 shown in figure 2.

Lump Mass 2	Cellar deck	Module deck	Module 1 – 6
Lump mass area [m ²]	2550	2550	14688
Total area[m ²]	4975	4325	14688
Ratio $\left[\frac{\text{m}^2}{\text{m}^2}\right]$	0,51256	0,58960	1,00
Total mass [ton]	8364,4	12409,1	4449,6
Lump mass weight [ton]	4287,3	7316,4	4449,6

$$x = \frac{(m_c \cdot x_c + m_{\text{mod}} \cdot x_{\text{mod}} + m_{1-6} \cdot x_{1-6})}{m_c + m_{\text{mod}} + m_{1-6}}$$

$$x = \underline{25,5\text{m}}$$

$$y = \frac{(m_c \cdot z_c + m_{\text{mod}} \cdot z_{\text{mod}} + m_{1-6} \cdot z_{1-6})}{m_c + m_{\text{mod}} + m_{1-6}}$$

$$y = \underline{23,89129\text{m}}$$

$$z = \frac{(m_c \cdot z_c + m_{\text{mod}} \cdot z_{\text{mod}} + m_{1-6} \cdot z_{1-6})}{m_c + m_{\text{mod}} + m_{1-6}}$$

$$z = \underline{14,2983\text{m}}$$